Assessment and Exploitation of the Minimum Current Harmonic Distortion Under Overmodulation in Five-Phase Induction Motor Drives

Martín Medina-Sánchez, Alejandro G. Yepes, *Senior Member, IEEE*, Óscar López, *Senior Member, IEEE*, and Jesús Doval-Gandoy, *Member, IEEE*

***Abstract*—This paper compares the most prominent overmodulation (OVM) techniques for five-phase induction motor drives with respect to the minimum current distortion (MCD) achievable. To attain a benchmark of the latter, two MCD OVM approaches are devised. Contrarily to previous strategies aimed at voltage distortion reduction/minimization, these MCD methods are focused on minimizing the harmonic stator copper loss (HSCL), thus minimizing the current total harmonic distortion (THD). One of these MCD strategies minimizes the HSCL while injecting only x–y harmonics. The other MCD method exploits α–β harmonic injection to further decrease the HSCL and to cover the whole OVM region. Moreover, the dual-mode OVM, which is one of the three-phase methods with the lowest distortion, is extended here for five-phase drives. The findings provide insight into how close the OVM methods are to the benchmark imposed by the MCD strategies. Notably, these MCD techniques yield a significant reduction of current THD, HSCL and peak current, especially for machines with negligible third-order space harmonic. The average switching losses are also decreased. Indications for real-time implementation of the MCD solutions are also given.**

***Index Terms*—Current distortion, five-phase drives, overmodulation (OVM), pulse width modulation (PWM), stator copper loss.**

ACRONYMS

Bs	Bolognani's.
CB	Carrier based.
DM	Dual mode.
HSCL	Harmonic stator copper loss.
MCD	Minimum current distortion.
MDE	Minimum distance error.
MPE	Minimum phase error.
MVD	Minimum voltage distortion.
NHSCL	Normalized harmonic stator copper loss.
OVM	Overmodulation.
PWM	Pulse width modulation.
THD	Total harmonic distortion.
WTHD	Weighted total harmonic distortion.

Manuscript received Month xx, 2xxx; revised Month xx, xxxx; accepted Month x, xxxx.

This work was supported in part by the Government of Galicia under the grants ED431F 2020/07 and GPC-ED431B 2020/03, in part by the Ministry of Science, Innovation and Universities under the Ramon y Cajal grant RYC2018-024407-I, and in part by the Spanish State Research Agency (AEI) under project PID2019-105612RB-I00/AEI/10.13039/501100011033. *(Corresponding author: Jesús Doval-Gandoy)*

The authors are with Applied Power Electronics Technology (APET) Research Group, CINTECX, Universidade de Vigo, Vigo 36310, Spain (e-mail: martindamian.medina@uvigo.es; agyepes@uvigo.es; olopez@uvigo.es; jdoval@uvigo.es).

This article has supplementary material provided by the authors and color versions of one or more figures available at http://ieeexplore.ieee.org.

Digital Object Identifier XXXX

I. INTRODUCTION

MULTIPHASE induction machines are emerging as an interesting solution due to a number of reasons. One of them is their inherent capability to withstand faults [1], [2], which is not normally present in the three-phase counterparts. Moreover, the higher phase number has proven to be efficient in the sense that the motor power is divided among more phases, therefore decreasing the per-phase current rating as well as the ohmic losses [3]. These features have made the multiphase machines an attractive alternative for applications such as electric vehicles and more-electric aircraft [4].

Regardless of the phase number, improving the dc-link utilization is beneficial in multiple ways [5]–[8]: extended speed range, tolerance to faults that decrease the dc-link voltage v_{dc}, reducing the electromagnetic noise and extra equipment for raising v_{dc}, etc. In this respect, five-phase machines offer interesting possibilities to exploit the dc-link voltage thanks to their extra degrees of freedom, which can be decomposed into three mutually orthogonal subspaces [2]: the α–β plane, also called torque-producing plane for sinusoidally distributed windings; the x–y plane; and the zero-sequence axis.

The noncurrent-producing zero-sequence voltage harmonics can be injected to increase the maximum reference modulation index M in the linear region of the PWM up to $1/\cos(\pi/10) \approx 1.052$ [9].[1] If the reference voltage surpasses the linear region, the PWM enters OVM. In OVM, besides zero-sequence harmonics, current-producing ones of the x–y and α–β planes may be injected in order to attain M [10]–[13]. For three-phase machines, only α–β harmonics, which cause torque ripple, are employed in OVM [14]. Nonetheless, torque pulsations can be prevented in five-phase motors by injecting just x–y harmonics up to a maximum M of 1.231 [12], [15]. This significant advantage over three-phase motors permits a greater modulation index without torque ripple.

In this regard, one of the oldest approaches to perform OVM in five-phase drives is based on combining just two

[1] M is computed as the ratio between the reference α–β fundamental voltage amplitude and $0.5v_{\mathrm{dc}}$.

voltage space vectors that are adjacent to the reference and of maximum magnitude in the α-β plane, i.e., two large space vectors [15]. A simple CB PWM solution equivalent to this method was devised in [6]. However, using only these two large space vectors causes considerable current distortion [12], aggravated by the low x–y impedance, given only by the stator resistance and leakage inductance [2]. These undesired currents may lead to machine damage [13], [16] and require greater sizing of the inverter [17], [18]. Many efforts have been done to alleviate this problem. In this respect, the use of special passive filters in [6], [19] helps to increase the x–y impedance with negligible α–β impedance, but increases the size and cost. Other strategies have been proposed to decrease the current distortion without passive filters, as described next.

On the one hand, there are OVM approaches that, while injecting only x–y harmonics (as those based on two large space vectors), are aimed at reducing to some extent [15], [20], [21] or minimizing [7], [12], [22] the x–y voltage. The latter feature is achieved by minimizing the instantaneous x–y voltage for each α–β reference. In this regard, the methods that rely on space-vector PWM [12], [22] are mainly based on the use of two large and two medium space vectors that are the nearest to the reference voltage. A CB equivalent strategy for minimizing x–y voltage, but less computationally intensive, was proposed in [7].

On the other hand, there are proposals that combine x–y and α–β voltage harmonic injection for different purposes in OVM. One of them is to increase M above 1.231 [7], [22]. In this sense, classical three-phase OVM methods have been adapted to five-phase drives: the so-called MPE, MDE and Bs. Another purpose is to reduce the HSCL when the integrity of the machine is compromised. In [13], if the ohmic loss tends to surpass its rated value, α–β distortion is injected (even for $M \leq 1.231$) while lowering x–y harmonic content, ensuring a safe drive operation.

Although many of the aforesaid methods are aimed to minimize the x–y voltage, none of them address the OVM problem from the perspective of minimizing the current THD, which implies minimizing the HSCL. Indeed, it has not been proven whether x–y voltage minimization implies current THD minimization. Since the former does not take into account the impedance difference between frequencies and between planes, it is reasonable to call into question this possible equivalence. Another important feature related to the current distortion, the peak current, has not been studied in detail yet in OVM either. Furthermore, it is unclear at this point if the solution from [13] (even when only α–β distortion is injected) is able to provide lower HSCL than those from [7]. Moreover, although some of the three-phase OVM solutions were extended to five phases in [7], the DM one [23], which is known to yield lowest HSCL and highest linearity between the reference and output modulation index up to the square waveform has not been adapted to five-phase drives yet.

For all these reasons, it can be stated that the actual minimum HSCL (current distortion) in five-phase drives under OVM, and the degree of closeness of the various solutions to such minimum, has not been properly assessed yet. Thus, this paper intends to fill these literature gaps with the following main contributions.

1) Extension of the three-phase DM OVM method to five-phase drives.
2) Development of two strategies that are aimed to attain the minimum HSCL, and therefore, the MCD, in OVM. One of these MCD strategies (MCD$_{xy}$) achieves it while injecting solely x–y voltage. The other MCD solution (MCD$_{\alpha\beta xy}$) includes suitable α–β harmonics to further decrease the HSCL as much as possible and also to cover the entire OVM region (up to the ten-step operation).
3) A comprehensive theoretical and experimental comparison is provided in terms of current distortion between the OVM methods (as well as the extended DM one) and the minimum achievable, given by the MCD strategies. HSCL, current THD and peak current are compared.

The rest of this article is organized as follows. Some essential background is addressed in Section II. The extension of the DM solution is explained in Section III. In Section IV, certain important figures of merit and the MCD OVM methods are introduced. Comparisons in terms of HSCL between the available OVM approaches and the minimum HSCL are given in Section V. Experimental results are presented in Section VI. Finally, the conclusions are summarized in Section VII.

II. Background

A. Vector Space Decomposition and Zero-Sequence Injection

The five-dimensional voltages/currents can be mapped into the α–β and x–y planes as well as in the zero-sequence axis, by using the vector space decomposition matrix $\mathbf{T}$, as

$$\begin{bmatrix} u_\alpha \\ u_\beta \\ u_x \\ u_y \\ u_{\text{zs}} \end{bmatrix} = \overbrace{\frac{2}{5}\begin{bmatrix} 1 & \cos\varphi & \cos 2\varphi & \cos 3\varphi & \cos 4\varphi \\ 0 & \sin\varphi & \sin 2\varphi & \sin 3\varphi & \sin 4\varphi \\ 1 & \cos 2\varphi & \cos 4\varphi & \cos 6\varphi & \cos 8\varphi \\ 0 & \sin 2\varphi & \sin 4\varphi & \sin 6\varphi & \sin 8\varphi \\ 1/2 & 1/2 & 1/2 & 1/2 & 1/2 \end{bmatrix}}^{\mathbf{T}} \begin{bmatrix} u_{\text{a}} \\ u_{\text{b}} \\ u_{\text{c}} \\ u_{\text{d}} \\ u_{\text{e}} \end{bmatrix} \tag{1}$$

where $\varphi = 2\pi/5$. In (1), u_m (for $m = \text{a}, \text{b}, \text{c}, \text{d}, \text{e}$) denotes the instantaneous values of the signals, either stator voltages v or currents i, while $U_{\alpha\beta} = u_\alpha + \text{j}u_\beta$ and $U_{xy} = u_x + \text{j}u_y$ are the space vectors in the α–β and x–y planes, respectively.

On the other hand, the harmonics in the zero-sequence axis can be used to enhance the dc-link utilization by injecting the so-called min-max voltage [24]

$$v_{\text{zs}} = -0.5(v_{\max} + v_{\min}) \tag{2}$$

where $v_{\max}$ ($v_{\min}$) is the instantaneous maximum (minimum) value of the set of the reference voltage signals v.

B. Linear and OVM Regions

A graphical representation of the OVM regions in the α–β plane is shown in Fig 1. This plane is divided into ten sectors (spanning $\pi/5$) by the 32 space vectors available in five-phase two-level inverters [22], [25]. Sinusoidal phase current (disregarding inverter and machine non-linearities) is possible if the circular trajectory described by the α–β reference voltage vector $V_{\alpha\beta}$ remains within the circle inscribed in the

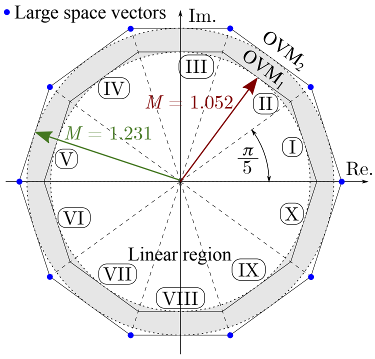

Fig. 1. Linear and OVM regions in the α–β plane of a five-phase inverter assuming circular $V_{\alpha\beta}$ trajectory.

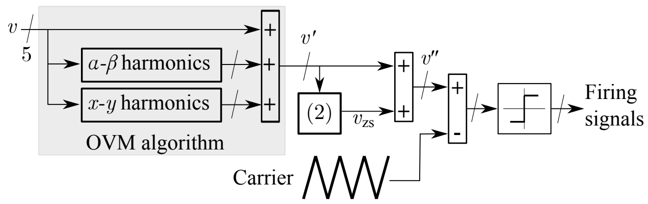

Fig. 2. OVM scheme with CB PWM implementation.

innermost decagon in Fig. 1 and the x–y reference voltage vector V_{xy} is zero. Hence, the maximum M in the linear region is 1.052 [9]. If the circular trajectory of $V_{\alpha\beta}$ surpasses the linear region, the modulator enters the OVM region [16].

The OVM region can be divided into two: OVM_1 and OVM_2. In OVM_1, depicted by the shaded area in Fig. 1, M can be achieved avoiding torque ripple by injecting just x–y voltage [26]. Under this approach, M can be increased up to 1.231 if the circular $V_{\alpha\beta}$ trajectory is within the circle inscribed in the outermost decagon in Fig. 1 [12], [15], whose vertices are the tips of large space vectors with magnitudes equal to $v_{\mathrm{L}} = 0.647v_{\mathrm{dc}}$ [9]. These space vectors divide the planes into ten sectors spanning $\pi/5$. Although x-y harmonic injection is in principle preferred in order to prevent torque pulsation, α–β harmonics may also be injected in OVM_1 if desired [13]. On the other hand, OVM_2 is beyond the inscribed circle in the outermost decagon. In this region, the injection of both α–β and x–y harmonics is mandatory [7].

Despite the fact that some OVM methods are based on space-vector PWM, they can be implemented through CB PWM following the scheme in Fig. 2 [7], [11] by using the vector space decomposition. The input of the OVM algorithm is the set of reference voltages v, which comprises five per-phase signals v_m. Subsequently, x–y and α–β (optionally) harmonics are injected to v, resulting in v'. Finally, the addition of v_{zs} to v' yields the modulating signals v'', which are compared with the carrier to produce the firing signals.

C. Existing OVM Methods for Five-Phase Drives

The noteworthy characteristics of the existing OVM strategies, to be compared later, are summarized in Table I. The new methods shown in Table I will be described in subsequent sections.

1) OVM With Only x–y Harmonic Injection: Among the methods based on x–y harmonic injection, the one that minimizes the instantaneous x–y voltage is remarkable, because it yields the MVD achieved so far [7], [12], [22]. This solution, referred to simply as MVD, is applicable only for OVM_1.

2) OVM With HSCL Control: The method in [13] adaptively adjusts the amount of x–y and α–β harmonics injected to the reference so that the rated stator copper loss of the machine is not exceeded. In this approach, two scenarios of operation are highlighted. In the first scenario the copper loss is smaller than its rated value and the algorithm adds to the reference just x–y voltage, which is in principle synthesized as that of using two large space vectors [9]. The strategy under this condition is called CB_{xy}. The second scenario occurs when the machine tends to exceed its safe ohmic loss, and to prevent it, the amount of x–y voltage is utmost reduced injecting instead the maximum degree of α–β harmonics (even in OVM_1) achievable by this technique. In this scenario, the solution is labeled $\mathrm{CB}_{\alpha\beta xy}$. Since α–β harmonics are permitted in $\mathrm{CB}_{\alpha\beta xy}$, this solution is also suitable for OVM_2.

3) Three-Phase OVM Methods Extended to Five-Phase Drives: In OVM_2, $V_{\alpha\beta}$ is distorted (when needed) resulting in the output voltage vector $V'_{\alpha\beta}$, which always remains within the outermost decagon in Fig. 1. To compute $V'_{\alpha\beta}$, the OVM methods for three-phase drives MPE [14], [27], MDE [14], [28] and Bs [29] were extended in [7] to five-phase drives. These already extended methods do not ensure that the output modulation index M', computed as the ratio of the fundamental amplitude of $V'_{\alpha\beta}$ and $0.5v_{\mathrm{dc}}$, is equal to M.

III. DM OVM for Five-Phase Drives

The three-phase DM solution [23], [27] comprises two modes of functioning where the fundamental amplitude of $V'_{\alpha\beta}$ matches that of $V_{\alpha\beta}$ up to the square waveform. Thus, $M' = M$ holds always and the operation of the inverter is linear in this sense (see Table I). This method, suitable for OVM_2, is extended in the following to five-phase drives.

A. Mode I ($1.231 \leq M < 1.252$)

In mode I, $V_{\alpha\beta}$ is lengthened while its phase angle $\theta = \omega_1 t$ remains unchanged. Thus, the $V'_{\alpha\beta}$ phase angle θ' is equal to θ. Remarkably, the $V'_{\alpha\beta}$ instantaneous magnitude $|V'_{\alpha\beta}|$ is bounded by the outermost decagon in Fig. 1. From the left side of Fig. 3(a), the reference angle α_{r} is the angle subtended by the intersection of the circular segment of the trajectory of $V'_{\alpha\beta}$ (red continuous line) with the decagon and the nearest large space vector. When $\alpha_{\mathrm{r}} = \pi/10$, the trajectory of $V'_{\alpha\beta}$ just touches the decagon and hence $V'_{\alpha\beta} = V_{\alpha\beta}$. Conversely, if $\alpha_{\mathrm{r}} = 0$, the trajectory of $V'_{\alpha\beta}$ overlaps with the decagon entirely, resulting in the maximum M' in mode I. Consequently, the amount by which $V_{\alpha\beta}$ has to be elongated is related to the value of α_{r}.

Therefore, M' is computed in advance as a function of α_{r} and stored in a look-up table. During operation, to match M' with M, the value of α_{r} is selected by using this look-up table. To calculate offline M' for the look-up table, the time-domain waveform of the real part of $V'_{\alpha\beta}$ is divided into six

TABLE I
SUMMARY OF OVM METHODS FOR FIVE-PHASE DRIVES AND CORRESPONDING ONES FOR THREE-PHASE DRIVES

Strategy	OVM region	Method description	References	
			Five-phase drives	Three-phase drives
MVD	OVM_1	Minimization of instantaneous x–y voltage	[7], [12], [22]	–
CB_{xy}	OVM_1	HSCL control: case of only x–y harmonics	[5], [13]	–
$\mathrm{CB}_{\alpha\beta xy}$	OVM_1/OVM_2	HSCL control: case of maximum α–β harmonics	[13]	–
MPE	OVM_2	Phase angle of $V'_{\alpha\beta}$ equal to that of $V_{\alpha\beta}$	[7]	[14], [27]
MDE	OVM_2	Minimization of the distance between $V_{\alpha\beta}$ and $V'_{\alpha\beta}$	[7], [22]	[14], [28]
Bs	OVM_2	Single mode of operation up to ten-step operation	[7]	[29]
DM	OVM_2	Two modes of operation with $M' = M$	Extended here	[23], [27]
MCD_{xy}	OVM_1	Minimization of HSCL with only x–y harmonics, i.e., J_{xy}	Devised here	–
$\mathrm{MCD}_{\alpha\beta xy}$	OVM_1/OVM_2	Minimization of HSCL with α–β and x–y harmonics, i.e., $J_{\alpha\beta xy}$	Devised here	–

segments, as shown in the right side of Fig. 3(a). This M' can be obtained by expanding the Fourier series [23]:

$$M'(\alpha_\mathrm{r}) = \frac{8}{\pi v_\mathrm{dc}} \sum_{k=1}^{6} \int_{\Theta_k} f_k \cos\theta d\theta \tag{3}$$

where Θ_k is the domain of the voltage equation f_k of the segment k. The functions f_k and their domains Θ_k are detailed in the Appendix. Solving (3) numerically yields the relation between M' and α_r depicted in Fig. 4(a). As can be seen therein, the upper limit of M' in mode I is 1.252. For modulation indices above this value, the DM enters mode II.

B. Mode II ($M \geq 1.252$)

Since the algorithm is symmetric with respect to the middle of each sector, the approach in mode II is detailed in the first half (shaded area in Fig. 3(b)) of sector I. While $V_{\alpha\beta}$ describes circular trajectories at constant angular frequency ω_1, $V'_{\alpha\beta}$ moves along the side of the decagon with the following strategies: while $\theta \leq \alpha_\mathrm{h}$, where α_h stands for the holding angle, $V'_{\alpha\beta}$ remains at the closest neighboring vertex to $V_{\alpha\beta}$; when $\theta > \alpha_\mathrm{h}$, $V'_{\alpha\beta}$ rotates from 0 to $\pi/10$ with a constant angular frequency so that $V'_{\alpha\beta}$ and $V_{\alpha\beta}$ are aligned when $\theta = \pi/10$. Thus, α_h controls how long $V'_{\alpha\beta}$ stays at the vertex.

Analogously to mode I, M' is computed as a function of α_h by dividing the time-domain waveform of the real part of $V'_{\alpha\beta}$ into six segments, as shown in the right part of Fig. 3(b). The voltage equations f_k and their domains Θ_k for mode II are also detailed in the Appendix. By solving numerically (3) with the corresponding values for mode II, the relation between α_h and M' is illustrated in Fig. 4(b). This relation is used to build the look-up table of mode II, which gives the value of α_h that ensures $M' = M$.

C. Overview of DM Implementation

Exploiting the symmetry with respect to the middle of each sector, the DM algorithm is summarized in Fig. 5 for the first half of sector I. In mode I, α_r is determined using the look-up table of Fig. 4(a). Then,

$$|V'_{\alpha\beta}| = \frac{v_\mathrm{L}\cos(\pi/10)}{\cos(\pi/10 - \alpha_\mathrm{r})} \tag{4}$$

while its phase angle $\theta' = \theta$. If $V'_{\alpha\beta}$ exceeds the decagon, its magnitude is bounded by the side of the latter as

$$|V'_{\alpha\beta}| = \frac{v_\mathrm{L}\cos(\pi/10)}{\cos(\pi/10 - \theta')}. \tag{5}$$

In mode II, the tip of $V'_{\alpha\beta}$ always matches the decagon side and hence $|V'_{\alpha\beta}|$ is given by (5) for any θ', which is established by the look-up table of Fig. 4(b) as follows: if $\theta \leq \alpha_\mathrm{h}$, then $\theta' = 0$; otherwise, $\theta' = \theta_1$ as in (A.3), in the Appendix. For $M > 1.273$, M' remains at 1.273 (ten-step operation).

In Fig. 6, M' versus M is illustrated for OVM_2. DM offers improved linearity compared with the OVM methods extended in [7] since M' equals M at all times up to the square waveform. As can be seen, Bs and MDE can reach the ten-step operation with poor linearity [7]. Conversely, MPE does not reach the square waveform and attains a maximum M' of 1.252 [7]. This value agrees with the maximum M' of mode I of DM. It is noteworthy that, for a given M', DM operating in mode I and MPE are fully equivalent since they maintain the condition $\theta' = \theta$. Therefore, the look-up table of Fig. 4(a) can also be used for linearization of MPE. For these reasons, MPE is disregarded hereinafter.

IV. MINIMUM HSCL FOR FIVE-PHASE DRIVES IN OVM

A. HSCL Due to Current Harmonics

The ohmic loss is caused by the stator current rms, which comprises the fundamental rms i_1 and the total harmonic rms i_ht. The former depends on the fundamental voltage and the developed electromagnetic torque and flux, and therefore, minimizing its losses is beyond the scope of this paper. Conversely, the HSCL provided by the current harmonics

$$HSCL = i_\mathrm{ht}^2 R_\mathrm{s} \tag{6}$$

where R_s is the stator resistance, may be minimized with a suitable OVM algorithm. Disregarding dc, even and zero-sequence components, the squared harmonic rms is

$$i_\mathrm{ht}^2 = \frac{1}{2}\sum_p \hat{i}_p^2 + \frac{1}{2}\sum_q \hat{i}_q^2 \tag{7}$$

where $\hat{i}_h$ (for $h = p, q$) denotes the amplitude of the hth current harmonic. For five-phase machines, the harmonic orders $p = 1 \pm 5l$ and $q = 2 \pm 5l$ (for $l = 1, 2, \dots$) are mapped in the α–β and x–y planes [30], respectively. If the p or

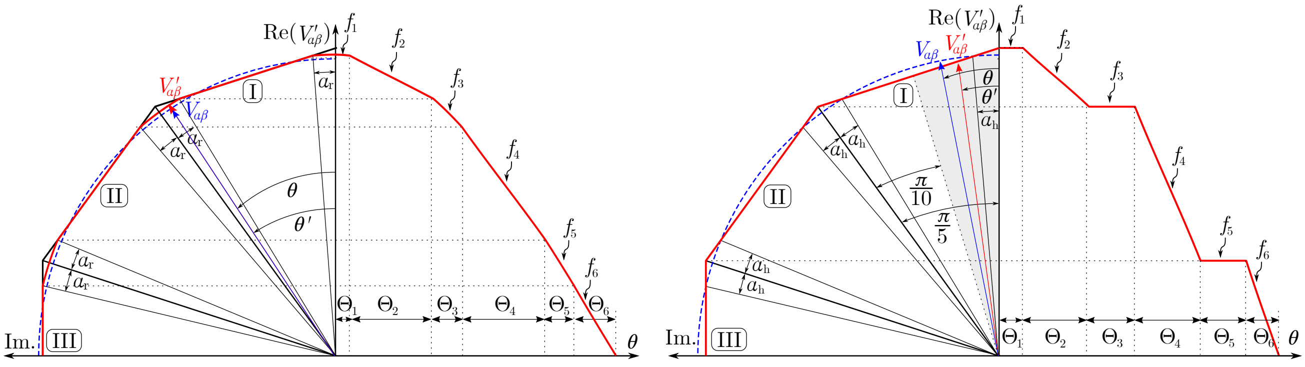

(a) (b)

Fig. 3. DM OVM strategy in (a) mode I and (b) mode II when $V_{\alpha\beta}$ enters the OVM$_2$ region in sector I. Left sides: $V_{\alpha\beta}$ trajectory (blue dashed line) and $V'_{\alpha\beta}$ trajectory (red continuous line) in the α–β plane. Right sides: time-domain waveform of the real component of $V'_{\alpha\beta}$.

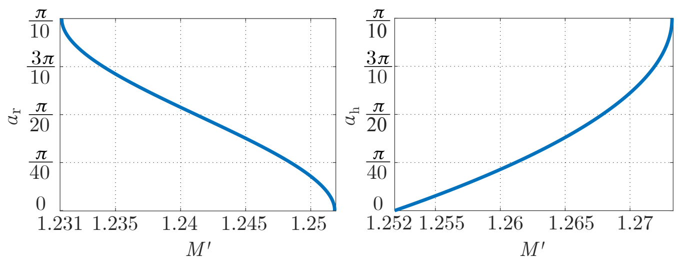

(a) (b)

Fig. 4. Look-up tables of DM OVM for five-phase drives. In (a) mode I $\alpha_{\rm r}$ and in (b) mode II $\alpha_{\rm h}$ are plotted versus M'.

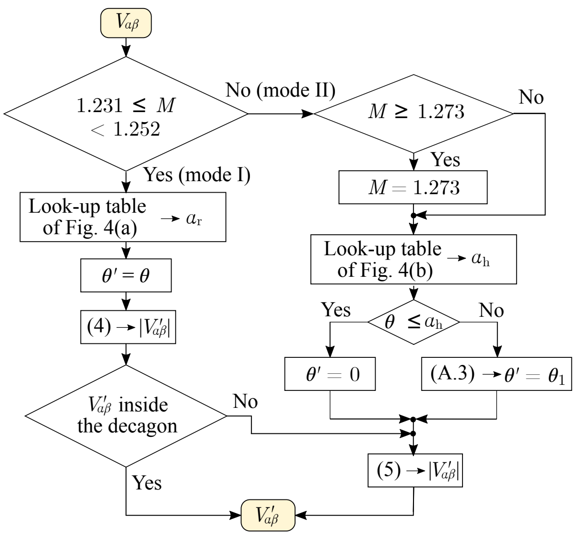

Fig. 5. Flowchart for real-time implementation of DM OVM for five-phase drives in OVM$_2$ and with $V_{\alpha\beta}$ in the first half of sector I.

q sign is positive or negative means that the corresponding harmonic space vector rotates in the same or in opposite direction compared with the α–β fundamental space vector. Even values of p and q are disregarded.

The currents $\hat{i}_h$ may be estimated from the voltage-harmonic amplitudes $\hat{v}_h$ by considering the impedances per plane. The α–β impedance $Z_{\alpha\beta}$, principally caused by the coupling between the stator and the rotor, can be considered as that of an RL circuit in steady state [31], [32]. The x–y impedance Z_{xy}

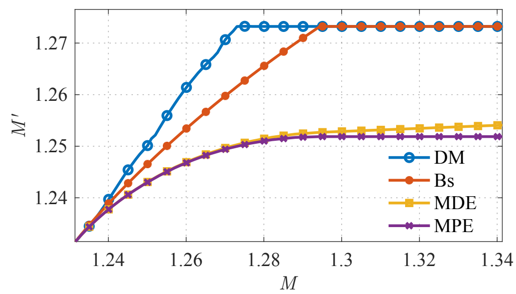

Fig. 6. M' versus M of three-phase OVM strategies extended to five-phase drives in the OVM$_2$ region.

is also derived from an RL circuit but without rotor coupling (assuming sinusoidally distributed windings [2]). Namely,

$$Z_{\alpha\beta}(p) \approx \sqrt{R_{\rm s}^2 + p^2\omega_1^2 L_\sigma^2};\, Z_{xy}(q) = \sqrt{R_{\rm s}^2 + q^2\omega_1^2 L_{\rm ls}^2} \quad (8)$$

where ω_1, L_σ and $L_{\rm ls}$ are the fundamental angular frequency, the transient stator inductance and the stator leakage inductance, respectively. Consequently, from (7) and (8),

$$i_{\rm ht}^2 = \frac{1}{2}\sum_p \frac{\hat{v}_p^2}{Z_{\alpha\beta}^2(p)} + \frac{1}{2}\sum_q \frac{\hat{v}_q^2}{Z_{xy}^2(q)}. \quad (9)$$

B. Estimation of Current Distortion With Distinction Between Planes

The current THD can be estimated in advance trough the voltage WTHD. The latter was originally devised for three-phase systems and its calculation as in [12], [21] underestimates the current THD for five-phase machines since it does not distinguish the impedance of both planes. Nevertheless, a more insightful voltage WTHD can be computed based on (9). Since usually OVM occurs when the machine rotates at relatively high frequency, it is reasonable to assume that $R_{\rm s}$ is much smaller than the inductive reactance. Thus, from (9),

$$i_{\rm ht}^2 = \frac{\hat{v}_1^2}{2\omega_1^2 L_\sigma^2} WTHD^2 \quad (10)$$

where $\hat{v}_1$ is the fundamental voltage amplitude, and

$$WTHD^2 = \overbrace{\frac{1}{\hat{v}_1^2}\sum_p \left(\frac{\hat{v}_p}{p}\right)^2}^{WTHD^2_{\alpha\beta}} + \overbrace{\frac{\delta^2}{\hat{v}_1^2}\sum_q \left(\frac{\hat{v}_q}{q}\right)^2}^{WTHD^2_{xy}}. \qquad (11)$$

The factor $\delta = L_\sigma/L_{\mathrm{ls}}$ in (11) reflects the relatively large distortion produced by the low impedance in x–y. In practical applications, machines are usually designed such that L_{ls} is roughly ten times smaller than L_σ [33], i.e., $\delta = 10$.

C. MCD OVM for Minimum HSCL

Minimizing the HSCL given by (6) for certain $\hat{i}_1$ and $\hat{v}_1$, implies minimizing i^2_{ht} in (9), and therefore, $WTHD^2$ in (11). Accordingly, the cost functions for the MCD OVM can be derived from (11) for simplicity and generality, or from (9) including the complete impedances for additional accuracy. Regardless of the choice, the MCD solution comprises two scenarios in which the cost functions J_{xy} and $J_{\alpha\beta xy}$ have to be minimized. If only x–y harmonics are injected in OVM$_1$, J_{xy} is minimized. To further reduce the HSCL in OVM$_1$, or to increase M' up to the ten-step operation in OVM$_2$, appropriate α–β harmonics (in addition to the x–y ones) are injected while minimizing $J_{\alpha\beta xy}$. Namely, from (11),

$$J_{xy} = \sum_q \left(\frac{\hat{v}_q}{q}\right)^2 ; J_{\alpha\beta xy} = \sum_p \left(\frac{\hat{v}_p}{p}\right)^2 + \delta^2 \sum_q \left(\frac{\hat{v}_q}{q}\right)^2 \qquad (12)$$

while from (9), including the actual impedances,

$$J_{xy} = \sum_q \frac{\hat{v}_q^2}{Z^2_{xy}(q)}; J_{\alpha\beta xy} = \sum_p \frac{\hat{v}_p^2}{Z^2_{\alpha\beta}(p)} + \sum_q \frac{\hat{v}_q^2}{Z^2_{xy}(q)}. \qquad (13)$$

To achieve $M' = M$ while minimizing the HSCL, the MCD OVM algorithms add harmonics to the per-phase reference voltage v_m, as depicted in Fig. 2. In general,

$$v'_m = v_m + \sum_p v_{m,p} + \sum_q v_{m,q} \qquad (14)$$

where

$$v_{m,p} = \hat{v}_p \cos(p\omega_1 t - \theta_{m,p}); v_{m,q} = \hat{v}_q \cos(q\omega_1 t - \theta_{m,q}) \qquad (15)$$

with $\theta_{m,p}$ ($\theta_{m,q}$) being the initial phase angle of the voltage harmonic $v_{m,p}$ ($v_{m,q}$). The procedure for determining suitable values of $\hat{v}_p$, $\hat{v}_q$, $\theta_{m,p}$, $\theta_{m,q}$ to minimize J_{xy}/$J_{\alpha\beta xy}$ from (12) or (13) is detailed in the following.

1) Optimization Problem: Taking advantage of symmetry, the optimization problem is defined for one of the five per-phase signals v'_m, e.g., v'_{a}, which is initialized to v_{a}. The signal v'_{a} is divided into N samples in one fundamental period T_1. Every sample $v'_{\mathrm{a}}(k)$ (for $k = 0, 1, 2, \ldots, N-1$) is considered as a variable that can be manipulated to minimize J_x for this phase. For a certain N value, harmonic orders up to $N/2$ are taken into account in the optimization. Among these harmonics, it is possible to consider that any odd harmonics up to a certain order $|h_{\mathrm{mx}}| \leq N/2$ may be injected, while all harmonic orders between $|h_{\mathrm{mx}}|$ and $N/2$ are restricted to zero. The higher $|h_{\mathrm{mx}}|$ is set, the lower the HSCL can be made and the higher M' can be reached, but the greater the sampling frequency needs to be in the real-time implementation (so that $|h_{\mathrm{mx}}|\omega_1$ is below the Nyquist frequency). Setting N so that $N/2 > |h_{\mathrm{mx}}|$ and forcing to zero the remaining harmonics makes it possible to implement the obtained solution with higher sampling frequencies than $2|h_{\mathrm{mx}}|\omega_1$ without unexpected behavior.

In addition, the following constraints must be imposed.

- If J_{xy} is being minimized, $\hat{v}_p$ is zero for every p.
- $\hat{v}_1$ in v'_{a} matches that of v_{a}, and hence $M' = M$.
- The even harmonics and dc component of v'_{a} are zero.
- The zero-sequence harmonics in v'_{a} are zero since they are optimally injected by v_{zs} afterward.
- Once v_{zs} is added to v'_{a}, the resulting signal v''_{a} must be between -1 and 1.

The signal v_{zs} as well as the amplitudes and initial phase angles of the voltage harmonics of v'_{a} are needed during the optimization process to impose these constraints. To compute v_{zs}, the other four phase signals v'_m (for $m = \mathrm{b, c, d, e}$) are required, which can be obtained by circularly shifting v'_{a} to the right by $N/5$ samples consecutively for each phase. Concerning the amplitudes and initial phase angles of the voltage harmonics of v'_{a}, they may be computed by applying the discrete Fourier transform to the N samples $v'_{\mathrm{a}}(k)$.

The outcomes of the minimization of J_{xy} and $J_{\alpha\beta xy}$ are hereinafter termed MCD$_{xy}$ and MCD$_{\alpha\beta xy}$, respectively (see Table I). It should be noticed that MCD$_{xy}$ does not inject α–β harmonics, whereas in MCD$_{\alpha\beta xy}$ these harmonics are allowed (even in OVM$_1$).

2) Online Implementation: For real-time implementation and to avoid minimizing J_{xy}/$J_{\alpha\beta xy}$ on-line, for each $M' = M$, the optimum values of $\hat{v}_p$, $\hat{v}_q$, $\theta_{\mathrm{a},p}$ and $\theta_{\mathrm{a},q}$ are stored in look-up tables. The remaining phase angles $\theta_{m,p}$ ($\theta_{m,q}$) for $m = \mathrm{b, c, d, e}$ could be determined by shifting $\theta_{\mathrm{a},p}$ ($\theta_{\mathrm{a},q}$) by the angle φ consecutively for each phase. Then, for a given $M' = M$, these optimum values are employed to inject the voltage harmonics to the voltage references v_m using (14).

However, a simpler implementation can be realized by using space vectors, as depicted in Fig. 7. Taking advantage of the fact that the phase angles of the voltage vectors of the α–β and x–y planes match $\theta_{\mathrm{a},p}$ and $\theta_{\mathrm{a},q}$, respectively,

$$\begin{aligned} V'_{\alpha\beta} &= V_{\alpha\beta} + \sum_p \hat{v}_p \exp[\mathrm{j}(p\theta - \theta_{\mathrm{a},p})] \\ V'_{xy} &= \sum_q \hat{v}_q \exp[\mathrm{j}(q\theta - \theta_{\mathrm{a},q})]. \end{aligned} \qquad (16)$$

Subsequently, the per-phase signals v' (see Fig. 2) are obtained by applying the inverse vector space decomposition matrix $\mathbf{T}^{-1}$ to $V'_{\alpha\beta}$ and V'_{xy}. An example of look-up tables containing the optimum amplitudes of the voltage harmonics versus M' is depicted in Fig. 8 for each MCD method. These strategies set the benchmarks of the minimum HSCLs in OVM for the subsequent assessments.

V. Comparison of the OVM Techniques With the Actual Minimum HSCL

In this section, the OVM methods for five-phase drives are assessed in terms of HSCL and voltage THD, with special

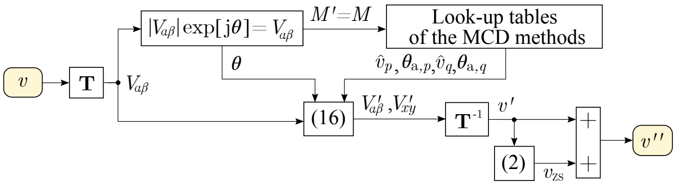

Fig. 7. Flowchart for real-time implementation of the MCD methods.

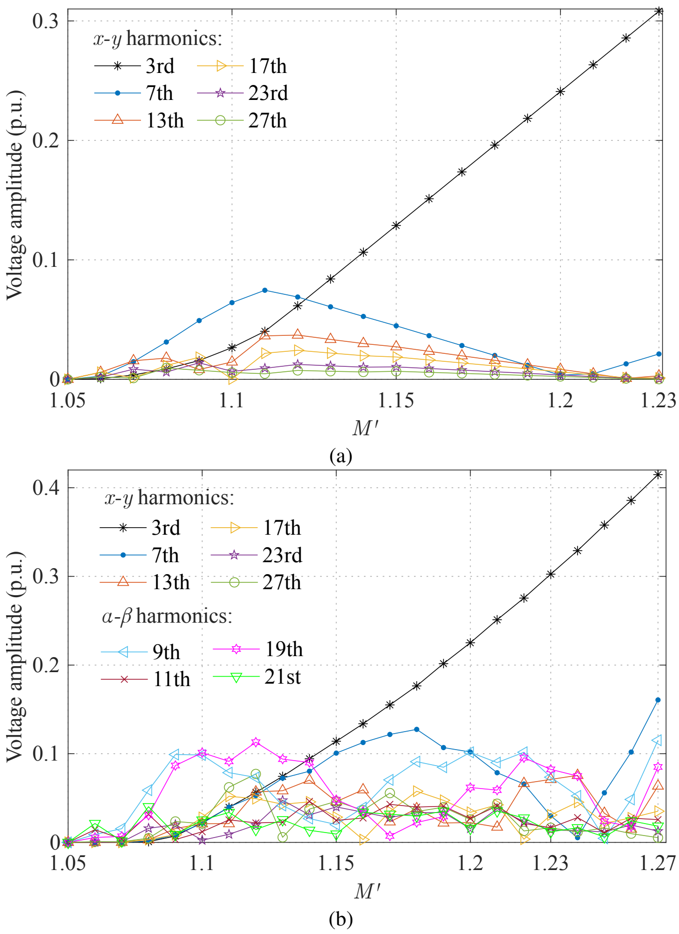

Fig. 8. Look-up tables containing the amplitudes (normalized by $0.5v_{\mathrm{dc}}$) of voltage harmonics versus $M' = M$ for the (a) MCD$_{xy}$ and (b) MCD$_{\alpha\beta xy}$ methods. The cost functions in (12) are minimized with the following parameters: $\delta = 10$, $N = 400$ and $|h_{\mathrm{mx}}| = 37$.

focus on the former. Moreover, the voltage WTHD, computed as in (11), is used as an estimation of current THD. For a clear comparison among the methods and without loss of generality, let us select the typical value $\delta = 10$ [33].

In particular, the minimum HSCL is achieved by solving the optimization problem of Section IV-C using the cost functions in (12), with the command *fmincon* (starting from multiple points) in Matlab. Moreover, N is set to 400 and the lower 37 current-producing harmonics are employed in the optimization problem (i.e., $|h_{\mathrm{mx}}| = 37$) so as to ensure that the HSCL is effectively minimized. The decrease in HSCL when optimizing more harmonics is negligible, whereas including fewer harmonics would raise the HSCL notably. The resulting look-up tables of the amplitudes of the voltage harmonics (up to the 27th one) of the MCD strategies match those in Fig. 8.

A Matlab/Simulink model with these MCD strategies, as well as the DM one, is included as supplementary material of the paper. Assuming the typical fundamental frequency of 50 Hz, and since $|h_{\mathrm{mx}}| = 37$, the subsequent assessments are valid for sampling frequencies above 3.7 kHz, which broadly include common sampling frequencies in OVM [5], [20]–[22].

A. *Assessment of HSCL and Voltage WTHD*

Calculation of the HSCL as in (6) depends of the machine parameters; for generality, a NHSCL [31], [32], [34] can be obtained by combining (6) and (10):

$$NHSCL = \frac{2\omega_1^2 L_\sigma^2}{\hat{v}_1^2 R_{\mathrm{s}}} HSCL = WTHD^2. \tag{17}$$

The strategies with only x–y voltage injection are compared first in OVM$_1$ in Fig. 9, as a function of the output modulation index M'. The minimum achievable NHSCL without torque ripple is provided by MCD$_{xy}$, as depicted in Fig. 9(a). MVD is relatively close to the minimum NHSCL for M' less than approximately 1.15, while for higher values of M', it matches the minimum. This observation is also in accordance with the estimation of current THD in Fig. 9(c). CB$_{xy}$ yields the maximum voltage WTHD, and hence the maximum NHSCL.

When α-β harmonics are added to the reference in OVM$_1$, the minimum NHSCL and current distortion is attained by MCD$_{\alpha\beta xy}$ for the entire OVM region (see Figs. 9 and 10). In this case, the injection of α–β voltage harmonics (with greater impedances) is exploited to further reduce the NHSCL compared with that of MCD$_{xy}$. This can be explained by comparing the amplitudes of the x–y voltage harmonics of MCD$_{xy}$ (in Fig. 8(a)) and MCD$_{\alpha\beta xy}$ (in Fig. 8(b)), where MCD$_{\alpha\beta xy}$ greatly reduces these troublesome harmonics, leading to an effective minimization of the NHSCL, and hence of the current THD. This drop of the current distortion, depicted in Fig. 9(c), is significant for M' below 1.12. Thus, optimal injection of α–β harmonics as MCD$_{\alpha\beta xy}$ does, improves the efficiency of the machine in OVM. Besides improving efficiency, these characteristics are crucial when the drive integrity is compromised if currents tend to exceed their safety ratings when only x–y voltage is injected [13]. Similarly, the reduction of x–y voltage by α–β harmonic injection in CB$_{\alpha\beta xy}$ decreases the NHSCL compared with CB$_{xy}$. Nonetheless, CB$_{\alpha\beta xy}$ yields more current distortion than MVD for M' greater than 1.07, as shown in Fig. 9(c); for M' below 1.07, it produces the same current distortion as MCD$_{\alpha\beta xy}$.

A comparison of the approaches in OVM$_2$, as a function of M', is also given in Fig. 10. The x–y harmonics of DM, MPE, MDE and Bs are computed as in MVD. In OVM$_2$, the minimum NHSCL is again imposed by MCD$_{\alpha\beta xy}$. DM and MDE equal the minimum NHSCL, while Bs and CB$_{\alpha\beta xy}$ are close to this value. It can be observed in Fig. 10(a) that, besides minimizing the current distortion, MCD$_{\alpha\beta xy}$ is able to reach an M' virtually equal to that of ten-step operation (1.273). If it is desired to attain such M' with even better accuracy, harmonic orders beyond the 37th may be included in the optimization process, at the cost of enlarging to some extent the size of the look-up tables for real-time implementation.

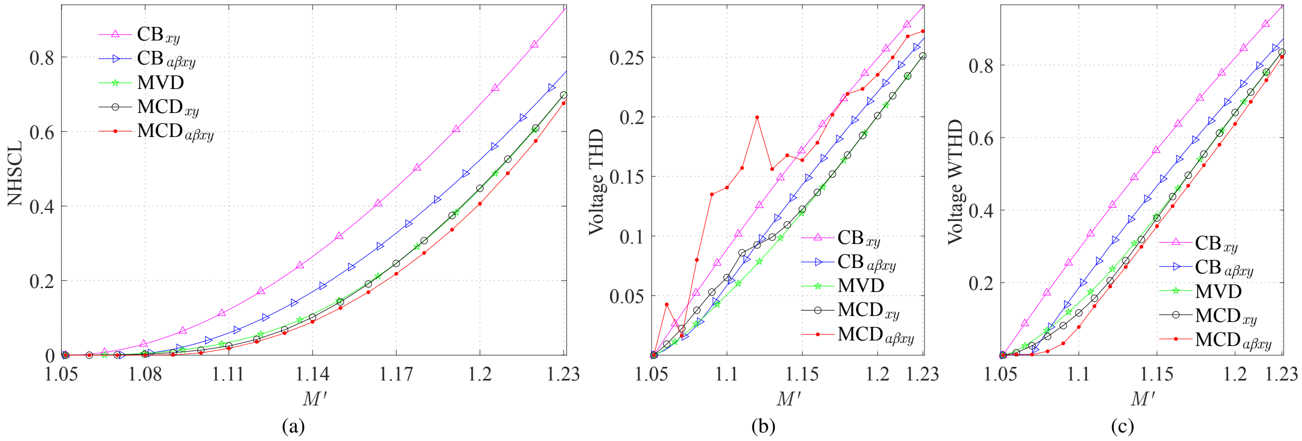

Fig. 9. Theoretical comparison of OVM strategies in the OVM$_1$ region in terms of (a) the NHSCL, (b) voltage THD and (c) voltage WTHD versus M'.

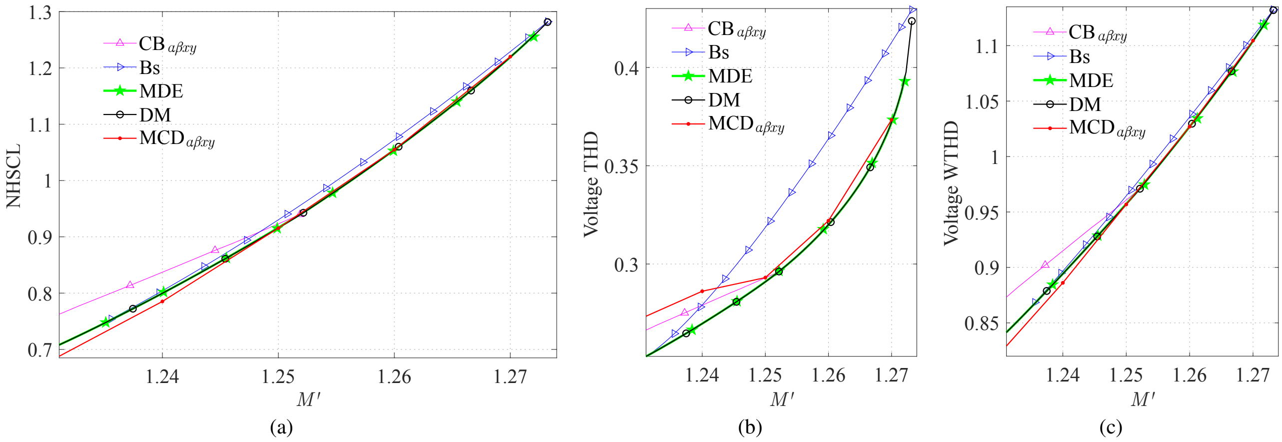

Fig. 10. Theoretical comparison of OVM strategies in the OVM$_2$ region in terms of (a) the NHSCL, (b) voltage THD and (c) voltage WTHD versus M'.

B. Voltage THD Comparison

Further observations can be done concerning the voltage THD of current-producing harmonics in Figs. 9(b) and 10(b). The minimum voltage THD is achieved by MVD and DM in the OVM$_1$ and OVM$_2$ regions, respectively. For M' over 1.15, MCD$_{xy}$ and MVD yield the same voltage THD. In contrast, MCD$_{\alpha\beta xy}$ and CB$_{xy}$ in OVM$_1$, as well as Bs and CB$_{\alpha\beta xy}$ in OVM$_2$, produce the largest voltage THD. Interestingly, the α–β harmonic injection in CB$_{\alpha\beta xy}$ reduces the voltage THD with respect to CB$_{xy}$, but this condition is reversed in MCD$_{\alpha\beta xy}$ as it produces more voltage THD than MCD$_{xy}$.

It is remarkable that reducing/minimizing the voltage THD is not equivalent to reducing/minimizing the current THD in OVM. In fact, the solution that produces the minimum current THD, i.e., MCD$_{\alpha\beta xy}$, yields the greatest voltage THD for certain M' values. This behavior may also be observed in MCD$_{xy}$, which only adds x–y voltage to the reference. The non-equivalence can be explained as follows: reducing the injection of low-order voltage harmonics (especially those of the x–y plane) mitigates the current distortion; instead of these harmonics, higher-order ones (with larger impedances) must be injected. The latter worsens the voltage THD. The reduction of x-y harmonics is particularly true for the third-order one, which produces the largest current distortion in OVM [5], [21]. As shown in Fig. 11, the amplitude of this harmonic is strongly related to the current distortion in Fig. 9(c). In addition, the reduction of this harmonic, besides alleviating ohmic losses [21], may decrease the peak current. The latter is beneficial in multiple ways, e.g., reduced sizing of the inverter switches [17], [18] or smaller x–y filters [6].

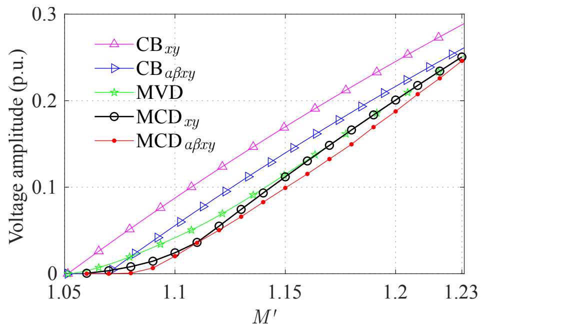

Fig. 11. Amplitude of the third voltage harmonic normalized by the fundamental component in the OVM$_1$ region.

VI. Experimental Results

Two experimental setups are devised to verify the theory. In the first setup (Section VI-A), the minimum HSCL in OVM is investigated in a five-phase induction motor directly connected to the inverter terminals (without extra inductors). This

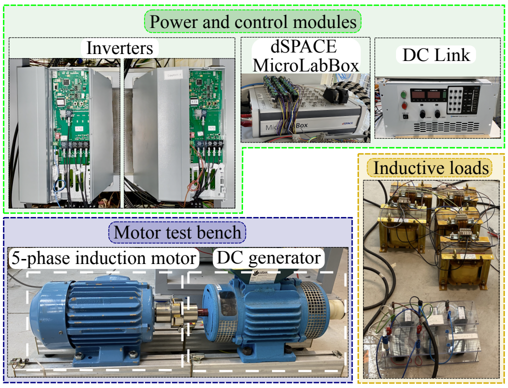

Fig. 12. Photographs of the experimental setups.

setup comprises two stages. The first stage (Section VI-A1) assumes that the motor has negligible space harmonics. The second stage (Section VI-A2) incorporates the actual harmonic impedances, measured to avoid unmodeled effects. In the second setup (Section VI-B), the induction machine is replaced by a set of inductive loads that are connected in such a fashion as to emulate the well-differentiated impedances per plane (α–β and x–y) of an ideal five-phase induction machine. Some pictures of these experimental setups are shown in Fig. 12.

Regardless of the experimental rig, the benchmark of the minimum HSCL in OVM is given by the MCD strategies. These minimum losses can be achieved by solving the optimization problem with the cost functions (12) or (13). Intuitive tests reveal the criteria for using one or the other cost function, as shown shortly. For real-time implementation of the MCD methods (see Section IV-C2), the solution of the optimization problem using $N = 400$ and $|h_{\mathrm{mx}}| = 37$ is stored in a look-up table for each M', with M' steps of 0.01. These settings provide adequate accuracy with an acceptable degree of complexity for the practical application.

The control unit used in the experiments is the dSPACE MicroLabBox with a sampling frequency of 10 kHz, which drives the inverter with a switching frequency of 10 kHz and dead time of 4 μs. The HSCL, current THD and voltage THD are determined by considering balanced harmonics up to the 49th, which are the most relevant and span a wider range than $|h_{\mathrm{mx}}|$. Moreover, oversampling and averaging are used to eliminate noise of higher frequencies in the current measurements [6], [13], [35], which is often due to electromagnetic interference and tends to introduce low-order harmonics by aliasing.

A. *Experiments With Five-Phase Induction Motor*

The motor parameters, assuming negligible space harmonics, are: two pole pairs, stator resistance $R_{\mathrm{s}} = 9.5\,\Omega$, magnetizing inductance $L_{\mathrm{m}} = 530$ mH, stator leakage inductance $L_{\mathrm{ls}} = 17$ mH, rotor resistance $R_{\mathrm{r}} = 7\,\Omega$, rotor leakage inductance $L_{\mathrm{lr}} = 35$ mH, transient stator inductance $L_{\sigma} = 52$ mH. Rated current of 1.27 A, rated voltage of 110 V and rated frequency of 50 Hz are assumed. As the effects of the torque load on the harmonic currents are negligible in OVM [11], without loss of generality, the tests are performed with no load to avoid overheating risk [13]. A dc generator is coupled to the motor to increase its inertia in order to reduce the effects of speed ripple.

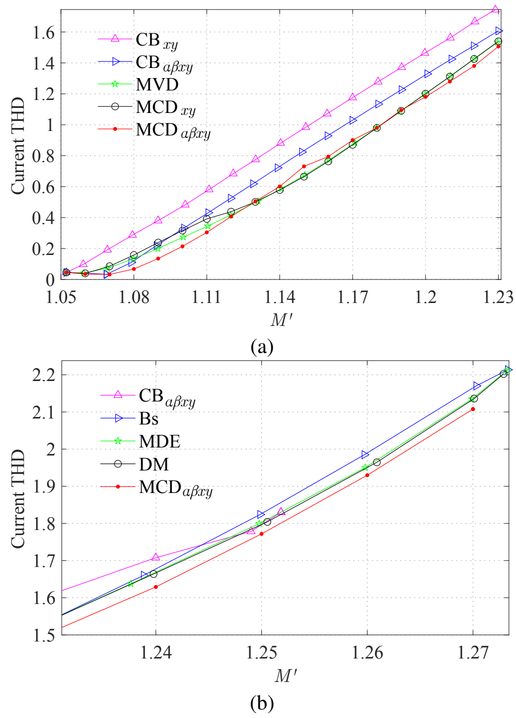

Fig. 13. Experimental results (of Section VI-A1) of the current THD of the induction motor in (a) OVM$_1$ and (b) OVM$_2$.

1) MCD Strategies Minimizing (12): A first design attempt of the MCD methods is made by minimizing (12). Minimizing J_{xy} for MCD$_{xy}$ does not require the motor parameters, whereas $J_{\alpha\beta xy}$ for MCD$_{\alpha\beta xy}$ needs δ (see (11)). With the given motor parameters, δ is roughly 3.

In the experiment, the motor is driven under open-loop V/f control. The fundamental voltage reference is maintained at 110 V, giving a fundamental current of 0.6 A. v_{dc} is decreased gradually from 293 V to 245 V, resulting in M' ranging from 1.05 to 1.27. The measurements are performed in steady state, with the motor running at rated frequency.

Fig. 13 shows the current THD versus M'. In OVM$_1$, the current THDs are essentially identical to those of Fig. 9(c), except for the MCD approaches. MCD$_{xy}$ produces slightly more current distortion than MVD for M' below 1.13; the same happens with MCD$_{\alpha\beta xy}$ for M' between 1.13 and 1.18. This unexpected behavior for the MCD solutions is solved next by considering the actual impedances of the motor. Thus, the impedances of the lower 37 current-producing harmonics are measured [36]. The first four ones of each plane are shown in Fig. 14. Therein, the measured impedances are compared with the theoretical ones, given by (8), under the assumption of negligible space harmonics. The difference of the actual versus the theoretical impedances is marginal, except for the third-order one. This impedance is substantially greater than the theoretical value as a result of undesired stator and rotor coupling [37]. Since this voltage harmonic is crucial in OVM, it is necessary to consider this non-ideal characteristic.

2) MCD Strategies Minimizing (13): The MCD strategies are now the outcome of minimizing (13) with a slight change:

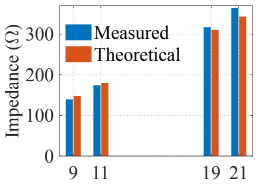

(a)

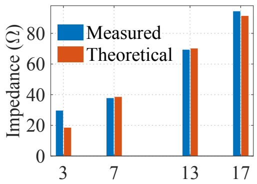

(b)

Fig. 14. Theoretical (sinusoidally distributed windings) and measured harmonic impedances of (a) α–β and (b) x–y planes at rated fundamental frequency of the motor in the experiments.

instead of using the theoretical impedances, the measured ones are employed. Thus, these MCD solutions address the non-ideal features of the motor. The experiment in Section VI-A1 is repeated for the new MCD methods. Additional results are shown for this case, which is of more interest.

If α–β harmonic injection is considered, now the minimum current THD is attained by $\mathrm{MCD}_{\alpha\beta xy}$ for every M' in OVM_1 (see Fig. 15(c)), which is in agreement with Fig. 9(c). $\mathrm{CB}_{\alpha\beta xy}$ equals such minimum for M' below approximately 1.07. Since the current THD is highly related to the HSCL, these relationships are the same in Fig. 15(a). Among the strategies with only x–y injection, the minimum HSCL is set by MCD_{xy}. The current THD of MVD equals that of MCD_{xy}, while CB_{xy} produces a noticeable current distortion.

As shown in Fig. 15(c), for M' below 1.13, $\mathrm{MCD}_{\alpha\beta xy}$ produces a considerable reduction of the current THD compared with MVD or even MCD_{xy}. Let us investigate this fact by analyzing the voltages and currents for a particular M', e.g., $M' = 1.10$, where the current THDs are 48.3%, 33.2%, 27.5%, 27.5% and 19.2% for CB_{xy}, $\mathrm{CB}_{\alpha\beta xy}$, MVD, MCD_{xy} and $\mathrm{MCD}_{\alpha\beta xy}$, respectively. For this M' (and also others), the inverter pole voltage references and phase currents are illustrated in Fig. 16 as well as their spectra in Fig. 17. As done in other papers [5]–[7], [13], the reference voltages are shown rather than voltage measurements because the former allow a better assessment of the harmonics injected by the OVM methods, without those due to converter non-linearities. Fig. 17(a) reveals that $\mathrm{MCD}_{\alpha\beta xy}$ avoids as much as possible the x–y third and seventh voltage harmonics, injecting instead α–β ones, which see much greater impedance. As predicted in the theoretical analysis, lowering these x–y harmonics not only mitigates the current distortion, but also reduces the value of the peak current, as can be appreciated in the experimental results depicted in Fig. 16. For this particular M', the peak-to-peak currents are 2.81 A, 2.50 A, 2.32 A, 2.31 A, and 2.13 A, for CB_{xy}, $\mathrm{CB}_{\alpha\beta xy}$, MVD, MCD_{xy} and $\mathrm{MCD}_{\alpha\beta xy}$, respectively; for other M' values in OVM_1 refer to Fig. 18(a), where its shape is strongly related to that of the current THD. Also for this M', the electromagnetic torque estimated from the machine voltage model by using the measured currents [38], is depicted in Fig. 19. This torque contains a second-order oscillation due to machine imbalance, which is present in all OVM techniques. The torque waveforms of $\mathrm{MCD}_{\alpha\beta xy}$ and $\mathrm{CB}_{\alpha\beta xy}$ are compared with that of MCD_{xy}, which does not inject α–β harmonics. $\mathrm{MCD}_{\alpha\beta xy}$ produces the largest torque pulsation of tenth order, but its amplitude is not appreciably greater than that of $\mathrm{CB}_{\alpha\beta xy}$ or the torque due to imbalance.

The voltage THD in Fig. 15(b) is consistent with that in Fig. 9(b), disregarding the MCD strategies, which now consider the actual impedances of the machine. The trajectories of the voltage references for certain M' values are depicted in Fig. 20, normalized by $0.5v_{\mathrm{dc}}$. The loci of the reference voltage in the α–β plane of CB_{xy}, MVD and MCD_{xy} describe circular trajectories. Conversely, $\mathrm{CB}_{\alpha\beta xy}$ and $\mathrm{MCD}_{\alpha\beta xy}$ distort the α–β voltage. For every M', the shape of the α–β voltage of $\mathrm{CB}_{\alpha\beta xy}$ resembles a decagon, while that of $\mathrm{MCD}_{\alpha\beta xy}$ is variable and dependent on M'. Concerning the x–y plane, the trajectories of CB_{xy} and $\mathrm{CB}_{\alpha\beta xy}$ are the largest ones. In addition, for M' above 1.15 the x–y loci of MCD_{xy} and MVD are essentially the same. The trajectories of $\mathrm{MCD}_{\alpha\beta xy}$ seem relatively larger, but actually produce the smallest current distortion.

From the results in OVM_2 of Fig. 21, the minimum HSCL is set again by $\mathrm{MCD}_{\alpha\beta xy}$. The current THDs of the strategies in OVM_2 are in line with those predicted in Fig. 10. From Fig. 21(c), the current distortion in OVM_2 is severe for all methods. This can be seen in detail in the spectrum, e.g., for $M' = 1.25$ in Fig. 22. A similar significant content of third current harmonic is noticeable in all strategies. Thus, the difference between the theoretical and measured impedance of the third harmonic is of minor importance in OVM_2. Consequently, the results of minimizing (12) in Fig. 13(b) are equivalent to those minimizing (13) in Fig. 21(c). Moreover, a considerable seventh harmonic and, to a lesser extent, the α–β harmonics, also contribute to the current distortion.

The peak-to-peak current in OVM_2 can be seen in Fig. 18(b). In general terms, DM and MDE yield the lowest peak amplitude, closely followed by $\mathrm{CB}_{\alpha\beta xy}$ and $\mathrm{MCD}_{\alpha\beta xy}$, while Bs produces the greatest amplitude.

Further remarks can be made regarding the inverter losses, which are mainly due to the conduction and switching losses. The conduction losses in one fundamental period are proportional to the current rms [39]. Hence, for a given fundamental current, reducing the harmonic distortion mitigates the conduction losses. In this sense, the behavior of the OVM methods in terms of conduction losses would be analogous to that concerning current THD in Figs. 15(c) and 21(c), with the smallest losses being reached by the MCD solutions. On the other hand, the switching losses are proportional to the average switching frequency [7], [28]. As depicted in Fig. 23, these losses are highly dependent on the OVM strategy. The increase in M' does not necessarily imply a reduction in switching frequency. For instance, CB_{xy} holds the switching frequency constant and virtually the same as that in the linear region of PWM. Conversely, the switching frequency of $\mathrm{MCD}_{\alpha\beta xy}$ gradually decays as M' raises. It is remarkable that $\mathrm{MCD}_{\alpha\beta xy}$ produces the minimum switching losses for almost the entire OVM_1 region. On the other hand, the commutations drop rapidly in OVM_2 and the strategies yield approximately the same switching frequencies.

B. Experiments With Inductive Loads

The case of a five-phase motor with negligible space harmonics (sinusoidal winding distribution [2]) is investigated in

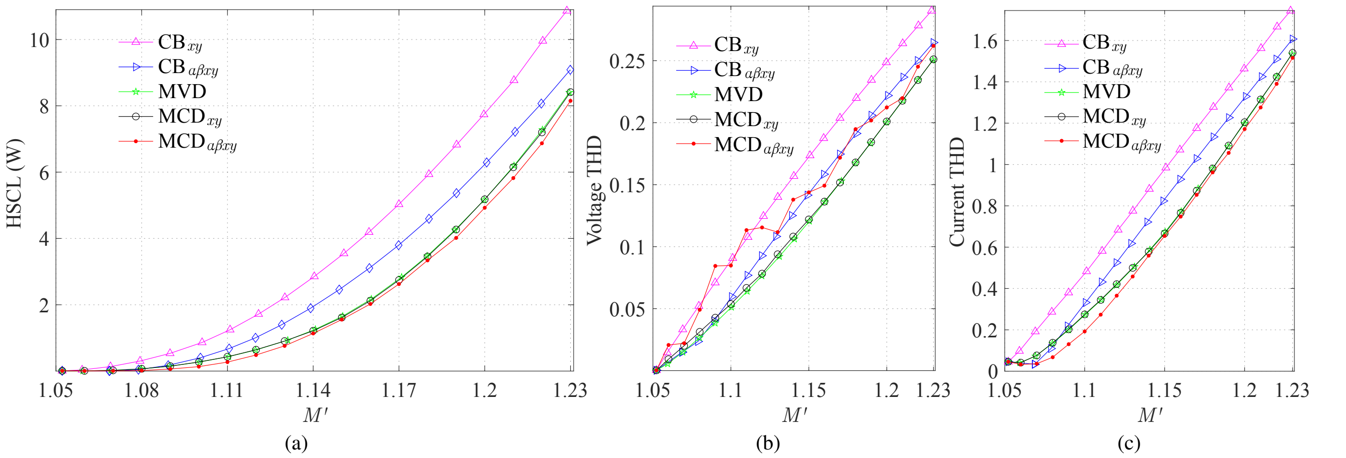

Fig. 15. Experimental results (of Section VI-A2) with the induction motor for the strategies in the OVM$_1$ region, in terms of (a) HSCL, (b) voltage THD and (c) current THD.

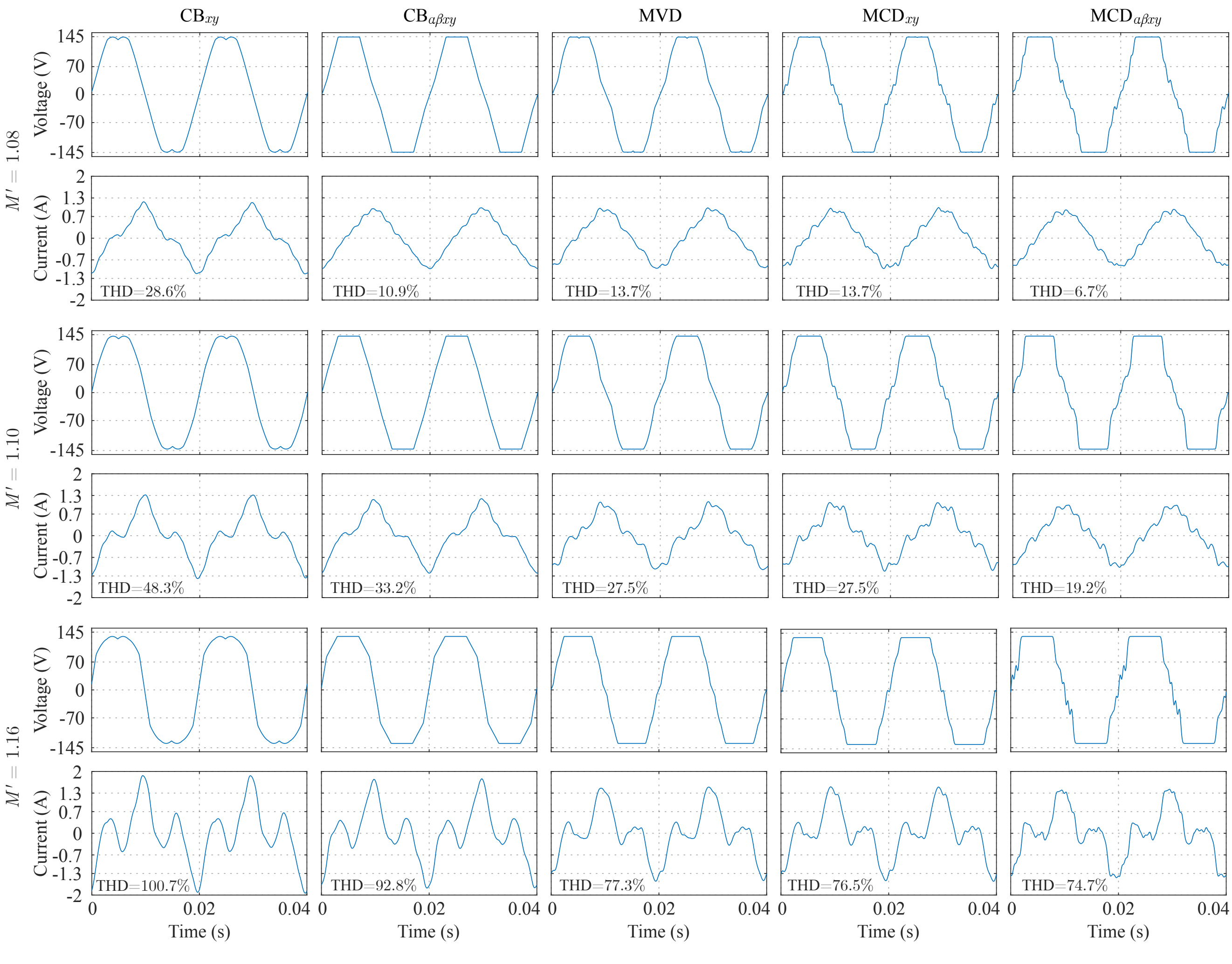

Fig. 16. Experimental results (of Section VI-A2) of the inverter output voltage reference and current in the time domain of the phase a of the induction motor, for $M' = 1.08$, $M' = 1.10$ and $M' = 1.16$.

this section. The impedances of this ideal motor are emulated through inductive loads that are connected so that the impedances of the α–β and x–y planes are well differentiated. This purpose is accomplished by using the five transformer-like passive filters employed in [6], but connected in such a way as to obtain an inductance of $95\,\mathrm{mH}$ in the α–β plane, and a negligible one in the x–y plane, instead of the opposite. Then, these filters are connected in series to five other star-

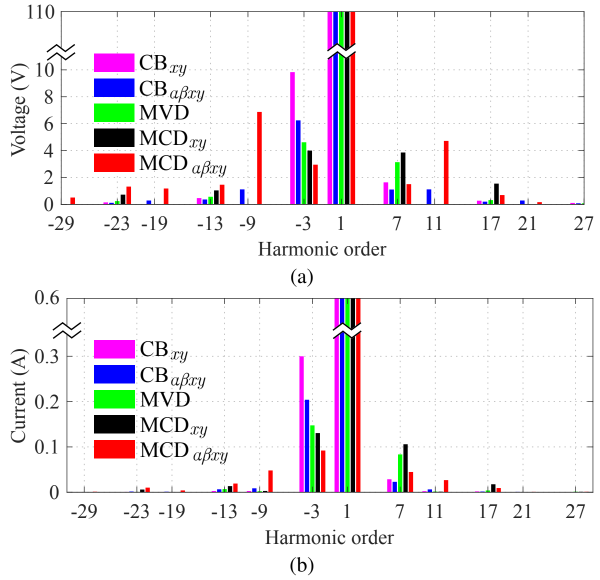

Fig. 17. Experimental results (of Section VI-A2) of the spectrum of (a) the output voltage reference and (b) stator current of the induction motor for an $M' = 1.10$ up to the 29th harmonic.

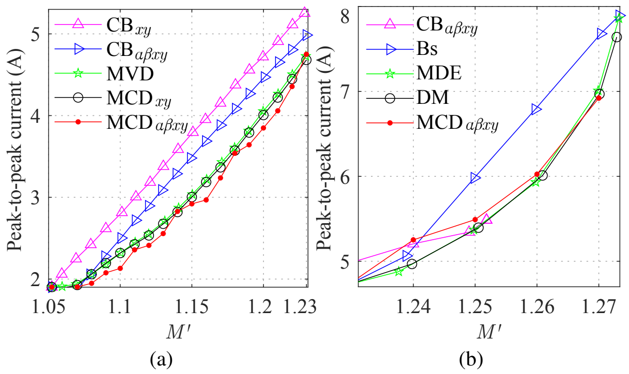

Fig. 18. Experimental results (of Section VI-A2) of the peak-to-peak current with the induction motor in (a) OVM$_1$ and (b) OVM$_2$ regions.

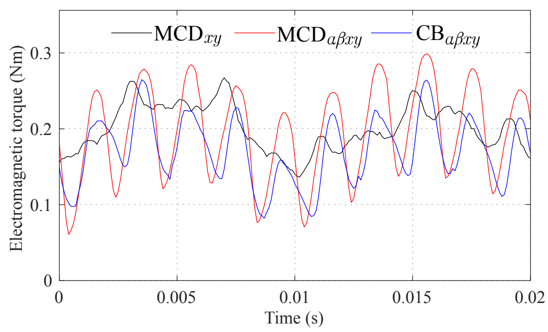

Fig. 19. Experimental results (of Section VI-A2) of the electromagnetic torque for $M' = 1.10$.

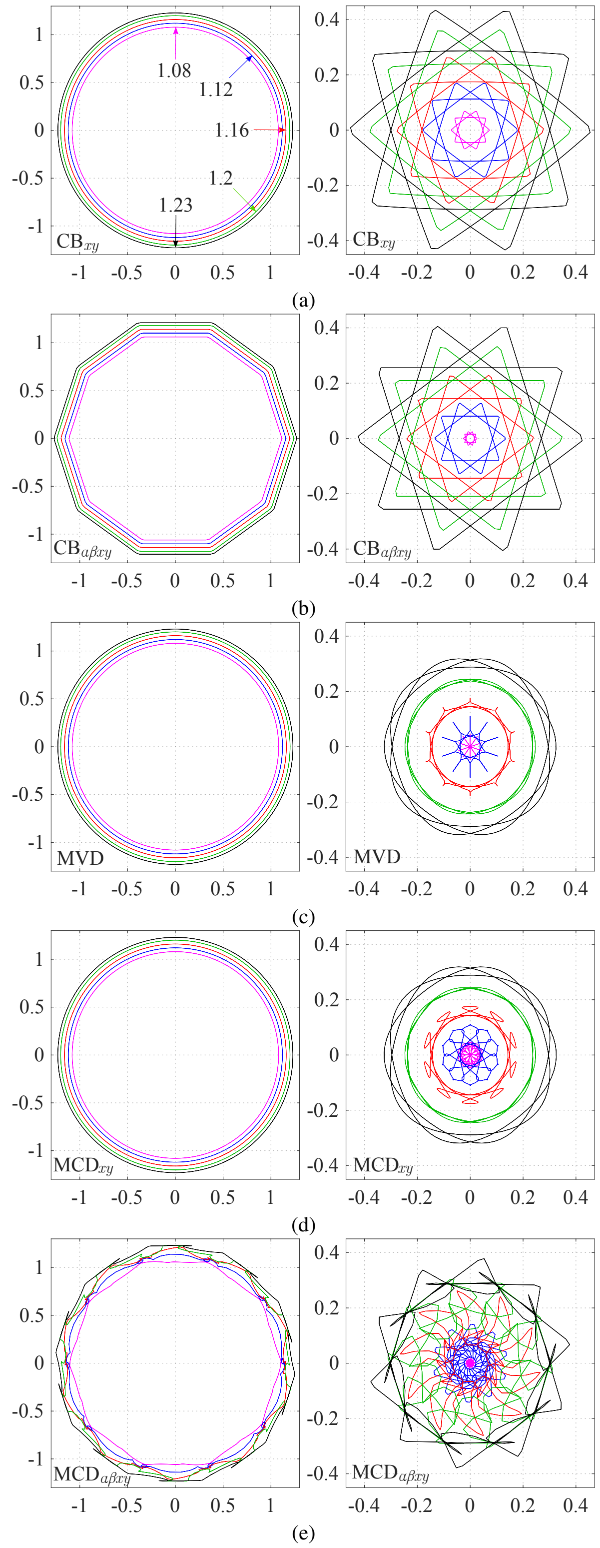

Fig. 20. Experimental results (of Section VI-A2) of the loci of reference voltage normalized by $0.5v_{\mathrm{dc}}$ using the induction motor for several M' values, in the α–β (left column) and x–y (right) planes. (a) CB$_{xy}$. (b) CB$_{\alpha\beta xy}$. (c) MVD. (d) MCD$_{xy}$. (e) MCD$_{\alpha\beta xy}$.

connected inductors of $10\,\mathrm{mH}$. This experimental scenario (see Fig. 12) gives a total inductance of $L_\sigma = 105\,\mathrm{mH}$ and $L_{\mathrm{ls}} = 10\,\mathrm{mH}$ in the α–β and x–y planes, respectively, and negligible resistance. For this setup δ is close to 10, and hence the MCD strategies used for the theoretical analysis in Section V are now evaluated. Thus, the look-up tables of the MCD schemes used in this experiment match those in Fig. 8 and included in the supplementary material.

Using open-loop control, the reference voltage is imposed with a fundamental voltage and frequency equal to $110\,\mathrm{V}$

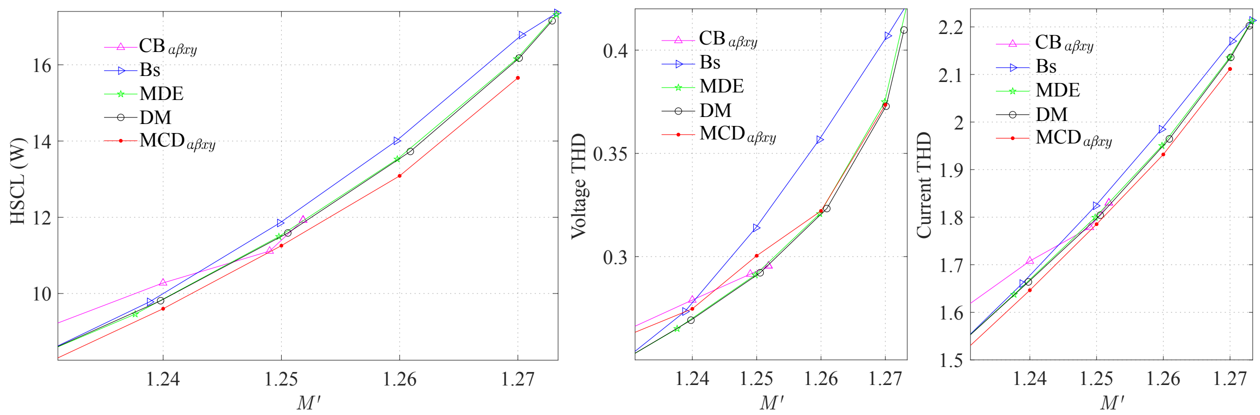

Fig. 21. Experimental results (of Section VI-A2) with the induction motor for the strategies in the OVM_2 region, in terms of (a) HSCL, (b) voltage THD and (c) current THD.

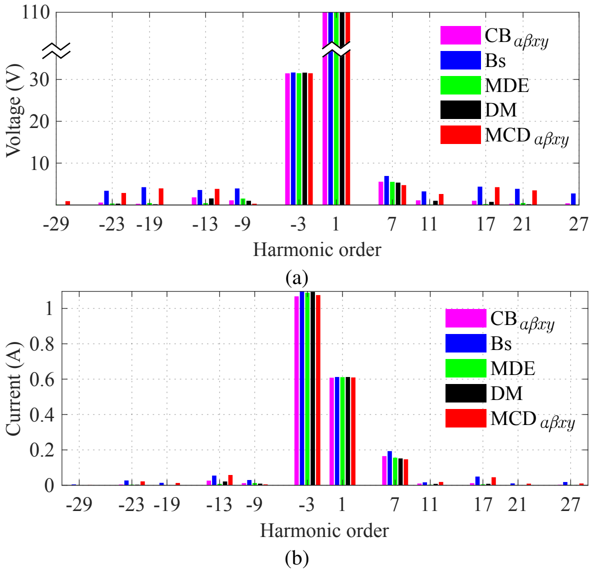

Fig. 22. Experimental results (of Section VI-A2) of the spectrum of the (a) output voltage reference and the (b) stator current of the induction machine for $M' = 1.25$ up to the 29th harmonic.

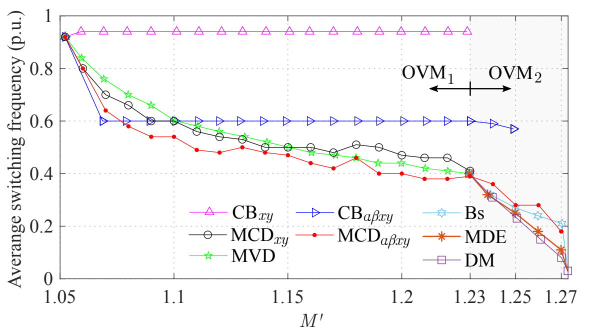

Fig. 23. Experimental results (of Section VI-A2) of the inverter average switching frequency for the entire OVM region with the induction motor.

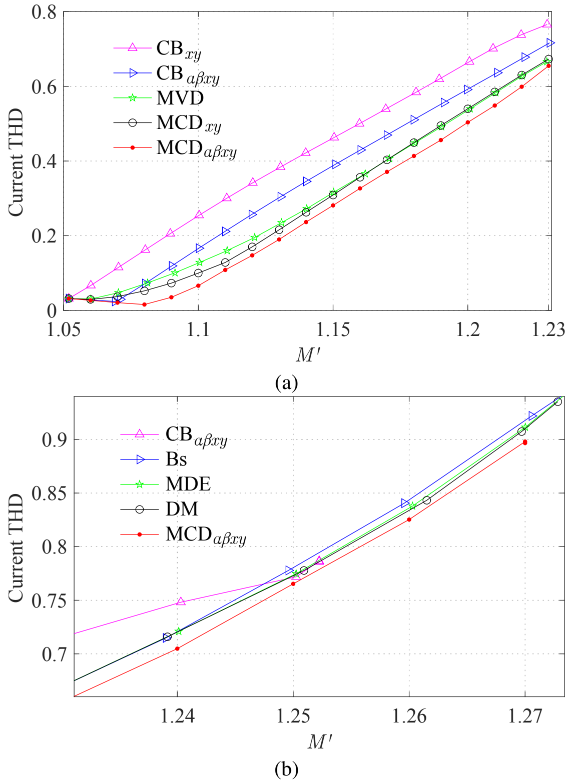

Fig. 24. Experimental results (of Section VI-B) of the current THD for inductive loads in (a) OVM_1 and (b) OVM_2.

and 100 Hz, respectively. $v_{\rm dc}$ drops progressively starting from 293 V, so M' ranges from 1.05 to 1.27. The voltage-reference THDs are the same as in Fig. 9(b) for OVM_1 and Fig. 10(b) for OVM_2. The resultant current THD is shown in Fig. 24, with the fundamental current remaining constant for each M' with a value of 1.7 A. Figs. 24(a) and 9(c) as well as Figs. 24(b) and 10(c) are essentially identical, which corroborates the entire theoretical analysis in Section V. It is worth remarking the accuracy of using the voltage WTHD based on (11) as an estimator of current THD.

If the space harmonics are negligible, the reduction of the current distortion by the MCD methods is enhanced. As expected from the theoretical analysis, MCD_{xy} now produces less current distortion than MVD for M' below 1.15, as can be seen in Fig. 24(a). To study these aspects, let us select the results for a particular M', again $M' = 1.10$. For

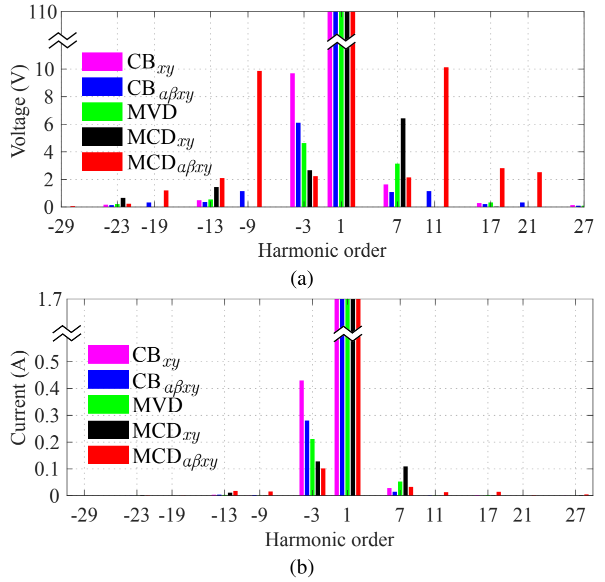

Fig. 25. Experimental results (of Section VI-B) of the spectrum of the (a) output voltage reference and the (b) phase current of the inductive loads for $M' = 1.10$ up to the 29th harmonic.

this M', the current THDs are 25.5%, 16.6%, 12.8%, 9.9% and 6.6% for CB_{xy}, $\text{CB}_{\alpha\beta xy}$, MVD, MCD_{xy} and $\text{MCD}_{\alpha\beta xy}$, respectively. The voltage spectrum for this M' is provided in Fig. 25(a). Compared with Fig. 17, MCD_{xy} produces a remarkable reduction of the x–y third-order voltage, injecting instead a relevant seventh-order one, which sees a relatively large impedance, as can be seen in Fig. 25(b). Although this aspect increases the voltage THD, it contributes to reducing the current distortion. This significant improvement with respect to Fig. 17 is made possible by the fact that, in absence of the third space harmonic, the difference between the impedances at the third and seventh harmonics is much larger. Also for this M', $\text{MCD}_{\alpha\beta xy}$ exploits the large impedance of α–β and not only reduces the third voltage harmonic, but also the seventh.

A marked reduction in the peak current is also noticeable for the MCD strategies, as depicted in Fig. VI-B, mainly due to decreasing the x–y third voltage harmonic (see Fig. 11). In this sense, $\text{MCD}_{\alpha\beta xy}$ exhibits a striking reduction and establishes the minimum current amplitude for the entire OVM region. In OVM_1, depicted in Fig. 26(a), it is worth noting that the peak amplitude of MCD_{xy} is virtually the same as that of $\text{MCD}_{\alpha\beta xy}$ for M' below 1.11 and less than that of MVD, especially for M' below 1.14. For the particular $M' = 1.10$, the peak-to-peak currents are 6.19 A, 5.74 A, 5.49 A, 5.27 A and 5.23 A for CB_{xy}, $\text{CB}_{\alpha\beta xy}$, MVD, MCD_{xy} and $\text{MCD}_{\alpha\beta xy}$, respectively. Remarkably, for many other M' in the OVM_1 the difference between $\text{MCD}_{\alpha\beta xy}$ and MVD is appreciably even greater. For instance, for $M' = 1.21$, the peak-to-peak currents are 7.81 A and 7.18 A for MVD and $\text{MCD}_{\alpha\beta xy}$, respectively. The advantages of $\text{MCD}_{\alpha\beta xy}$ also hold in OVM_2 region, illustrated in Fig. 26(b); e.g., for $M' = 1.24$ the peak-to-peak currents are 8.75 A, 8.62 A, 8.60 A, 8.55 A and 8.24 A for $\text{CB}_{\alpha\beta xy}$, Bs, MDE, DM and $\text{MCD}_{\alpha\beta xy}$, respectively.

Based on the experimental comparison, the most relevant features of each OVM method (see Table I) are summarized in Table II and Table III for OVM_1 and OVM_2, respectively.

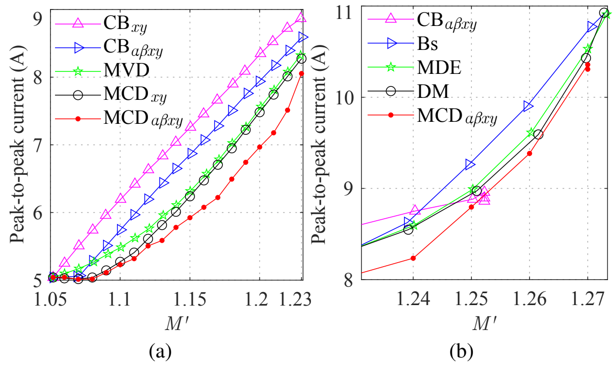

Fig. 26. Experimental results (of Section VI-B) of the peak-to-peak current with inductive loads in (a) OVM_1 and (b) OVM_2.

TABLE II
COMPARISON OF OVM METHODS IN OVM_1

Strategy	Minimum current THD	Minimum voltage THD	Current peak
CB_{xy}	No	No	Very high
$\text{CB}_{\alpha\beta xy}$	Just if $M' \leq 1.07$	No	High
MVD	Just if $M' \geq 1.15$	Yes	Medium
MCD_{xy}	Yes	Just if $M' \geq 1.15$	Low
$\text{MCD}_{\alpha\beta xy}$	Yes	No	Very low

TABLE III
COMPARISON OF OVM METHODS IN OVM_2

Strategy	Minimum current THD	Minimum voltage THD	Current peak	$M' = M$
Bs	No	No	Very high	No
$\text{CB}_{\alpha\beta xy}$	No	No	High	Just if $M' \leq 1.25$
MDE	No	Yes	Medium	No
DM	No	Yes	Low	Yes
$\text{MCD}_{\alpha\beta xy}$	Yes	No	Very low	Yes

VII. CONCLUSIONS

The most notable and recent OVM strategies for five-phase drives have been studied in terms of current distortion, compared with the minimum achievable. The main contributions are the following.

1) The DM solution, which is one of the most important strategies for OVM in three-phase machines, has been extended here to five-phase drives. DM allows exploiting the dc link up to the square waveform with relatively low current distortion. Unlike previous three-phase methods extended before, this strategy offers improved linearity between the reference and output modulation indices.
2) Two MCD strategies have been devised here to provide the benchmark of the actual minimum HSCL and current THD in OVM, both for machines with negligible and non-negligible space harmonics. These strategies are the outcome of minimizing figures of merit that have been improved to differentiate the impedances between

frequencies and between planes for five-phase machines. If only x–y voltage is injected, the MCD is established by MCD_{xy} for modulation indices between 1.052 and 1.231. On the other hand, α–β voltage harmonics, which see large impedances, are exploited to further reduce the HSCL by $\mathrm{MCD}_{\alpha\beta xy}$, besides extending the modulation indices beyond 1.23 with also enhanced linearity as DM.
3) A detailed study of the performance of existing OVM strategies has provided insightful information about the degree of closeness of said strategies to the benchmark of the minimum HSCL (current distortion). This was carried out through theory and experiments.

From the results of this study, some remarkable findings are highlighted in terms of HSCL.

- For modulation indices below 1.231, MVD is closest to MCD_{xy}, while CB_{xy} produces substantial current distortion and is far from MCD_{xy}. Moreover, $\mathrm{CB}_{\alpha\beta xy}$ equals the current distortion of $\mathrm{MCD}_{\alpha\beta xy}$ for modulation indices below 1.07, while for higher modulation indices it produces even more distortion than MVD. On the other hand, for modulation indices above 1.231, Bs and $\mathrm{CB}_{\alpha\beta xy}$ yield more current distortion than DM and MDE, and the latter group is the nearest to $\mathrm{MCD}_{\alpha\beta xy}$.
- The minimization of voltage THD does not imply the minimization of current THD. This fact holds true even if only x–y harmonics are injected, especially if the effect of the third-order space harmonic on the impedance is negligible. Although MVD and DM/MDE produce the minimum voltage THD, the minimum current THD is attained by the new MCD strategies, despite introducing significant voltage distortion.

Moreover, other important findings regarding the current peak are listed subsequently.

- Broadly speaking, from the results with the induction motor for modulation indices below 1.231, the solutions can be listed in descending order of peak magnitude as CB_{xy}, $\mathrm{CB}_{\alpha\beta xy}$, MVD, MCD_{xy} and $\mathrm{MCD}_{\alpha\beta xy}$. The descending order for modulation indices above 1.231 is as follows: Bs, $\mathrm{CB}_{\alpha\beta xy}$, $\mathrm{MCD}_{\alpha\beta xy}$, MDE and DM. In the test emulating a machine with negligible space harmonics (using inductive loads), the minimum current amplitude was imposed by $\mathrm{MCD}_{\alpha\beta xy}$ for the entire OVM region.
- It has been evidenced that the peak amplitude is strongly influenced by the current distortion of the x–y harmonics, especially by the third one. Therefore, reducing these harmonics as much as possible contributes to decreasing the peak current.

The improvements provided by the new MCD methods make it possible to decrease the HSCL, peak current and inverter losses compared with previous OVM techniques, thus enhancing efficiency and reducing the required sizing and overheating risk of the machine and inverter, especially for relatively low modulation indices within OVM. For example, for a modulation index of 1.10, the current THD and the peak-to-peak current were reduced from 12.8% and 5.49 A (of MVD) to 9.9% and 5.27 A (of MCD_{xy}) or to 6.6% and 5.23 A (of $\mathrm{MCD}_{\alpha\beta xy}$), respectively.

Due to the interesting features of the MCD strategies for five-phase drives, future work should be done extending them to other multiphase drives. Moreover, the performance of such strategies with closed-loop control, during transients, voltage-drop faults or parameter excursions may also be addressed.

Appendix

In mode I of DM OVM for five-phase drives, the voltage equations of the segments in the time-domain waveform of the real part of $V'_{\alpha\beta}$, depicted in Fig. 3(a), can be written as

$$\begin{aligned}
f_1 &= \frac{v_\mathrm{L}\cos(\pi/10)}{\cos(\pi/10-\alpha_\mathrm{r})}\cos\theta, \theta\in\Theta_1=[0,\alpha_\mathrm{r})\\
f_2 &= \frac{v_\mathrm{L}\cos(\pi/10)}{\cos(\pi/10-\theta)}\cos\theta, \theta\in\Theta_2=\left[\alpha_\mathrm{r},\frac{\pi}{5}-\alpha_\mathrm{r}\right)\\
f_3 &= \frac{v_\mathrm{L}\cos(\pi/10)}{\cos(\pi/10-\alpha_\mathrm{r})}\cos\theta, \theta\in\Theta_3=\left[\frac{\pi}{5}-\alpha_\mathrm{r},\frac{\pi}{5}+\alpha_\mathrm{r}\right)\\
f_4 &= \frac{v_\mathrm{L}\cos(\pi/10)}{\cos(3\pi/10-\theta)}\cos\theta, \theta\in\Theta_4=\left[\frac{\pi}{5}+\alpha_\mathrm{r},\frac{2\pi}{5}-\alpha_\mathrm{r}\right)\\
f_5 &= \frac{v_\mathrm{L}\cos(\pi/10)}{\cos(\pi/10-\alpha_\mathrm{r})}\cos\theta, \theta\in\Theta_5=\left[\frac{2\pi}{5}-\alpha_\mathrm{r},\frac{2\pi}{5}+\alpha_\mathrm{r}\right)\\
f_6 &= \frac{v_\mathrm{L}\cos(\pi/10)}{\cos(\pi/2-\theta)}\cos\theta, \theta\in\Theta_6=\left[\frac{2\pi}{5}+\alpha_\mathrm{r},\pi/2\right).
\end{aligned}\tag{A.1}$$

Similarly, the voltage equations for mode II in Fig. 3(b) are

$$\begin{aligned}
f_1 &= v_\mathrm{L}, \theta\in\Theta_1=[0,\alpha_\mathrm{h})\\
f_2 &= \frac{v_\mathrm{L}\cos(\pi/10)}{\cos(\pi/10-\theta_1)}\cos\theta_1,\ \theta\in\Theta_2=\left[\alpha_\mathrm{h},\frac{\pi}{5}-\alpha_\mathrm{h}\right)\\
f_3 &= v_\mathrm{L}\cos\frac{\pi}{5},\ \theta\in\Theta_3=\left[\frac{\pi}{5}-\alpha_\mathrm{h},\frac{\pi}{5}+\alpha_\mathrm{h}\right)\\
f_4 &= \frac{v_\mathrm{L}\cos(\pi/10)}{\cos(3\pi/10-\theta_2)}\cos\theta_2, \theta\in\Theta_4=\left[\frac{\pi}{5}+\alpha_\mathrm{h},\frac{2\pi}{5}-\alpha_\mathrm{h}\right)\\
f_5 &= v_\mathrm{L}\cos\frac{2\pi}{5}, \theta\in\Theta_5=\left[\frac{2\pi}{5}-\alpha_\mathrm{h},\frac{2\pi}{5}+\alpha_\mathrm{h}\right)\\
f_6 &= \frac{v_\mathrm{L}\cos(\pi/10)}{\cos(\pi/2-\theta_3)}\cos\theta_3, \theta\in\Theta_6=\left[\frac{2\pi}{5}+\alpha_\mathrm{h},\pi/2\right)
\end{aligned}\tag{A.2}$$

where

$$\theta_1=\frac{\theta-\alpha_\mathrm{h}}{1-\dfrac{10\alpha_\mathrm{h}}{\pi}};\theta_2=\frac{\theta-3\alpha_\mathrm{h}}{1-\dfrac{10\alpha_\mathrm{h}}{\pi}};\theta_3=\frac{\theta-5\alpha_\mathrm{h}}{1-\dfrac{10\alpha_\mathrm{h}}{\pi}}.\tag{A.3}$$

References

[1] A. G. Yepes, O. Lopez, I. Gonzalez-Prieto, M. J. Duran, and J. Doval-Gandoy, “A comprehensive survey on fault tolerance in multiphase ac drives, part 1: General overview considering multiple fault types,” *Machines*, vol. 10, no. 3, Mar. 2022.

[2] E. Levi, “Multiphase electric machines for variable-speed applications,” *IEEE Trans. Ind. Electron.*, vol. 55, no. 5, pp. 1893–1909, May 2008.

[3] E. Levi, R. Bojoi, F. Profumo, H. A. Toliyat, and S. Williamson, “Multiphase induction motor drives—A technology status review,” *IET Electr. Power Appl.*, vol. 1, no. 4, pp. 489–516, Jul. 2007.

[4] F. Barrero and M. J. Duran, “Recent advances in the design, modeling and control of multiphase machines—Part I,” *IEEE Trans. Ind. Electron.*, vol. 63, no. 1, pp. 449–458, Jan. 2016.

[5] A. G. Yepes and J. Doval-Gandoy, “Simple carrier-based PWM for prolonged high dc-link utilization for symmetrical and asymmetrical n-phase ac drives,” *IEEE Trans. Power Electron.*, vol. 36, no. 8, pp. 8696–8712, Aug. 2021.

[6] A. G. Yepes, J. Doval-Gandoy, and H. A. Toliyat, "Improvement in dc-link utilization with reduced current and torque deterioration for five-phase drives by combination of circulating-current filters and simple carrier-based PWM based on closed-form expressions," *IEEE Trans. Ind. Electron.*, vol. 68, no. 2, pp. 960–971, Feb. 2021.
[7] L. Vancini, M. Mengoni, G. Rizzoli, G. Sala, L. Zarri, and A. Tani, "Carrier-based PWM overmodulation strategies for five-phase inverters," *IEEE Trans. Power Electron.*, vol. 36, no. 6, pp. 6988–6999, Jun. 2021.
[8] H. Mahlfeld, T. Schuhmann, R. Döbler, and B. Cebulski, "Impact of overmodulation methods on inverter and machine losses in voltage-fed induction motor drives," in *Proc. ICEM*, Nov. 2016, pp. 1064–1070.
[9] A. Iqbal and S. Moinuddin, "Comprehensive relationship between carrier-based PWM and space vector PWM in a five-phase VSI," *IEEE Trans. Power Electron.*, vol. 24, no. 10, pp. 2379–2390, Oct. 2009.
[10] Y. Zhu, W. Gu, K. Lu, and Z. Wu, "Vector control of asymmetric dual three-phase PMSM in full modulation range," *IEEE Access*, vol. 8, pp. 104 479–104 493, 2020.
[11] C. Zhou, G. Yang, and J. Su, "PWM strategy with minimum harmonic distortion for dual three-phase permanent-magnet synchronous motor drives operating in the overmodulation region," *IEEE Trans. Power Electron.*, vol. 31, no. 2, pp. 1367–1380, Feb. 2016.
[12] G. Carrasco and C. Silva, "Space vector PWM method for five-phase two-level VSI with minimum harmonic injection in the overmodulation region," *IEEE Trans. Ind. Electron.*, vol. 60, no. 5, pp. 2042–2053, May 2013.
[13] A. G. Yepes and J. Doval-Gandoy, "Overmodulation method with adaptive x-y current limitation for five-phase induction motor drives," *IEEE Trans. Ind. Electron.*, vol. 69, no. 3, pp. 2240–2251, Mar. 2022.
[14] Y.-C. Kwon, S. Kim, and S.-K. Sul, "Six-step operation of PMSM with instantaneous current control," *IEEE Trans. Ind. Appl.*, vol. 50, no. 4, pp. 2614–2625, Jul./Aug. 2014.
[15] A. Iqbal and E. Levi, "Space vector modulation schemes for a five-phase voltage source inverter," in *Proc. EPE*, Sep. 2005, pp. 1–12.
[16] S. Halasz, "Overmodulation region of multi-phase inverters," in *Proc. EPE-PEMC*, Sep. 2008, pp. 682–689.
[17] T. J. dos Santos Moraes, N. K. Nguyen, F. Meinguet, and E. Semail, "Fault tolerant dual-motor drives: Sizing of power electronic," in *Proc. ECPEA*, Sep. 2015, pp. 1–10.
[18] T. Dos Santos Moraes, N. K. Nguyen, E. Semail, F. Meinguet, and M. Guerin, "Dual-multiphase motor drives for fault-tolerant applications: Power electronic structures and control strategies," *IEEE Trans. Power Electron.*, vol. 33, no. 1, pp. 572–580, Jan. 2018.
[19] E. A. Klingshirn, "Harmonic filters for six-phase and other multiphase motors on voltage source inverters," *IEEE Trans. Ind. Appl.*, vol. IA-21, no. 3, pp. 588–594, May/Jun. 1985.
[20] J. Prieto, F. Barrero, M. J. Duran, S. Toral Marin, and M. A. Perales, "SVM procedure for n-phase VSI with low harmonic distortion in the overmodulation region," *IEEE Trans. Ind. Electron.*, vol. 61, no. 1, pp. 92–97, Jan. 2014.
[21] F. Bu, T. Pu, Q. Liu, B. Ma, M. Degano, and C. Gerada, "Four-degree-of-freedom overmodulation strategy for five-phase space vector pulsewidth modulation," *IEEE J. Emerg. Sel. Top. Power Electron.*, vol. 9, no. 2, pp. 1578–1590, Apr. 2021.
[22] M. J. Duran, J. Prieto, and F. Barrero, "Space vector PWM with reduced common-mode voltage for five-phase induction motor drives operating in overmodulation zone," *IEEE Trans. Power Electron.*, vol. 28, no. 8, pp. 4030–4040, Aug. 2013.
[23] D.-C. Lee and G.-M. Lee, "A novel overmodulation technique for space-vector PWM inverters," *IEEE Trans. Power Electron.*, vol. 13, no. 6, pp. 1144–1151, Nov. 1998.
[24] E. Levi, D. Dujic, M. Jones, and G. Grandi, "Analytical determination of dc-bus utilization limits in multiphase VSI supplied ac drives," *IEEE Trans. Energy Convers.*, vol. 23, no. 2, pp. 433–443, Jun. 2008.
[25] J. Kelly, E. Strangas, and J. Miller, "Multiphase space vector pulse width modulation," *IEEE Trans. Energy Convers.*, vol. 18, no. 2, pp. 259–264, Jun. 2003.
[26] A. Iqbal and E. Levi, "Space vector PWM techniques for sinusoidal output voltage generation with a five-phase voltage source inverter," *Electr. Power Compon. Syst.*, vol. 34, no. 2, pp. 119–140, 2006.
[27] J. Holtz, W. Lotzkat, and A. Khambadkone, "On continuous control of PWM inverters in the overmodulation range including the six-step mode," *IEEE Trans. Power Electron.*, vol. 8, no. 4, pp. 546–553, Oct. 1993.
[28] A. F. Abouzeid, J. M. Guerrero, A. Endemaño, I. Muniategui, D. Ortega, and F. Briz, "Assessment of overmodulation strategies for ac drives considering harmonics content and switching losses," in *Proc. IEEE IEMDC*, Jun. 2021, pp. 1–6.
[29] S. Bolognani and M. Zigliotto, "Novel digital continuous control of SVM inverters in the overmodulation range," *IEEE Trans. Ind. Appl.*, vol. 33, no. 2, pp. 525–530, Mar./Apr. 1997.
[30] A. G. Yepes, J. Doval-Gandoy, and H. A. Toliyat, "Multifrequency current control for n-phase machines including antiwindup and distortion-free saturation with full dc-bus utilization," *IEEE Trans. Power Electron.*, vol. 34, no. 10, pp. 9891–9905, Oct. 2019.
[31] P. Stumpf and S. Halász, "Optimization of PWM for the overmodulation region of two-level inverters," *IEEE Trans. Ind. Appl.*, vol. 54, no. 4, pp. 3393–3404, Jul./Aug. 2018.
[32] S. Halasz, I. Varjasi, and A. Zacharov, "Overmodulation strategies of inverter-fed ac drives," in *Proc. PCC*, vol. 3, Aug. 2002, pp. 1346–1351 vol.3.
[33] P. Krause, O. Wasynczuk, and S. Sudhoff, *Analysis of Electric Machinery and Drive Systems*, W.-I. Press, Ed., 2002.
[34] P. Stumpf, K. Bándy, and S. Halász, "Space vector based investigation of overmodulation region of inverter fed multiphase ac drives," in *Proc. PEMC*, May 2021, pp. 506–513.
[35] S. N. Vukosavic, L. S. Peric, and E. Levi, "Digital current controller with error-free feedback acquisition and active resistance," *IEEE Trans. Ind. Electron.*, vol. 65, no. 3, pp. 1980–1990, Sep. 2018.
[36] A. G. Yepes, J. A. Riveros, J. Doval-Gandoy, F. Barrero, O. López, B. Bogado, M. Jones, and E. Levi, "Parameter identification of multiphase induction machines with distributed windings—Part 1: Sinusoidal excitation methods," *IEEE Trans. Energy Convers.*, vol. 27, no. 4, pp. 1056–1066, Dec. 2012.
[37] L. A. Pereira, C. C. Scharlau, L. F. A. Pereira, and J. F. Haffner, "General model of a five-phase induction machine allowing for harmonics in the air gap field," *IEEE Trans. Energy Convers.*, vol. 21, no. 4, pp. 891–899, Dec. 2006.
[38] C.-C. Wang and C.-H. Fang, "Sensorless scalar-controlled induction motor drives with modified flux observer," *IEEE Trans. Energy Convers.*, vol. 18, no. 2, pp. 181–186, Jun. 2003.
[39] E. P. Wiechmann, P. Aqueveque, R. Burgos, and J. Rodriguez , " On the efficiency of voltage source and current source inverters for high-power drives," *IEEE Trans. Ind. Electron.*, vol. 55, no. 4, pp. 1771–1782, Apr. 2008.

Martin Medina-Sánchez received the M.Sc. degree in automation and control engineering from the Escuela Superior Politécnica de Chimborazo, Ecuador, in 2017. He is currently working toward the Ph.D degree in electrical engineering with the Applied Power Electronics Technology Research Group (APET), Universidade de Vigo.

His research interests include multiphase drives and power electronics.

Alejandro G. Yepes (Senior Member, IEEE) received the M.Sc. and Ph.D. degrees in electrical engineering from Universidade de Vigo, Vigo, Spain, in 2009 and 2011, respectively. Since 2008, he has been working with the Applied Power Electronics Technology Research Group, Universidade de Vigo. From August 2016 to June 2018, he stayed with the Department of Electrical and Computer Engineering, Texas A&M University, College Station, TX, USA, after which he returned to Universidade de Vigo. His research interests are in the areas of ac power conversion, with special focus, currently, on multiphase drives.

Oscar López (Senior Member, IEEE) received the M.Sc. and Ph.D. degrees in electrical engineering from the University of Vigo, Vigo, Spain, in 2001 and 2009, respectively.

Since 2004, he has been an Assistant Professor at the University of Vigo. He is a member of the Applied Power Electronics Technology Research Group, University of Vigo. His research interests include the areas of ac power switching converters technology.

Jesús Doval-Gandoy (Member, IEEE) received the M.Sc. and Ph.D. degrees in electrical engineering from the Polytechnic University of Madrid, Madrid, Spain, and from Universidade de Vigo, Vigo, Spain, in 1991 and 1999, respectively. He is a Professor and the Head of the Applied Power Electronics Technology Research Group (APET), Universidade de Vigo.

His research interests are in the areas of ac power conversion.